

1 **EpCAM<sup>+</sup>CD73<sup>+</sup> mark epithelial progenitor cells in postnatal human lung and is**  
2 **associated with pathogenesis of pulmonary disease including lung**  
3 **adenocarcinoma**

4  
5 Limei Wang<sup>1,2</sup>, Patrick Dorn<sup>1</sup>, Cedric Simillion<sup>3</sup>, Laurène Froment<sup>1,2</sup>, Sabina  
6 Berezowska<sup>4</sup>, Stefan A. Tschanz<sup>5</sup>, Beat Haenni<sup>5</sup>, Fabian Blank<sup>2,6</sup>, Carlos Wotzkow<sup>6</sup>,  
7 Ren-Wang Peng<sup>1,2</sup>, Thomas M. Marti<sup>1,2</sup>, Peter K. Bode<sup>7</sup>, Ueli Moehrlen<sup>8</sup>, Ralph A.  
8 Schmid<sup>1,2†</sup> and Sean R.R. Hall<sup>1,2†</sup>  
9

10 <sup>1</sup>Division of General Thoracic Surgery, Inselspital, Bern University Hospital, Bern,  
11 Switzerland

12 <sup>2</sup>Department of BioMedical Research, University of Bern, Switzerland

13 <sup>3</sup>Interfaculty Bioinformatics, University of Bern, Switzerland

14 <sup>4</sup>Institute of Pathology, University of Bern, Bern, Switzerland

15 <sup>5</sup>Institute of Anatomy, University of Bern, Switzerland

16 <sup>6</sup>DCR Live Imaging Core, University of Bern, Switzerland

17 <sup>7</sup>Department of Pathology and Molecular Pathology, University Hospital Zurich,  
18 Switzerland

19 <sup>8</sup>Department of Pediatric Surgery, University Children's Hospital, Zurich, Switzerland

20  
21 †Address correspondence to Sean R.R. Hall or Ralph A. Schmid, <sup>1</sup>Division of General  
22 Thoracic Surgery, Inselspital, Bern University Hospital and Department of BioMedical  
23 Research, University of Bern, Murtenstrasse 50, 3008 Bern, Switzerland

24 Tel. +41 031 632 2300

25 Fax. +41 031 632 2327

26 Email: Sean.Hall@insel.ch or Ralph.Schmid@insel.ch  
27

28  
29 **Funding:** LW is a doctoral student supported by a 4-year China Scholarship Council  
30 award. Laser scanning microscopy imaging was funded by the R'Equip grant from the  
31 Swiss National Science Foundation Nr. 316030\_145003.  
32

33 **Running Title:** CD73 progenitor cells in human lung.  
34

35 **Abstract word count:** 250  
36

37 Lung injury in mice induces mobilization of discrete subsets of epithelial progenitor cells  
38 to promote new airway and alveolar structures. However, whether similar cell types exist  
39 in human lung remains unresolved. Using flow cytometry, we identified a distinct cluster  
40 of cells expressing epithelial cell adhesion molecule (EpCAM), a cell surface marker  
41 expressed on epithelial progenitor cells, enriched in the ecto-5'-nucleotidase CD73 in  
42 unaffected postnatal human lung resected from pediatric patients with congenital lung  
43 lesions. Within the EpCAM<sup>+</sup>CD73<sup>+</sup> population, a small subset co-express integrin β4 and  
44 HTII-280. This population remained stable with age. Spatially, EpCAM<sup>+</sup>CD73<sup>+</sup> cells were  
45 positioned along the basal membrane of respiratory epithelium and alveolus next to  
46 CD73<sup>+</sup> cells lacking EpCAM. Expanded EpCAM<sup>+</sup>CD73<sup>+</sup> cells give rise to pseudostratified  
47 epithelium in 2D air-liquid interface or a clonal 3D organoid assay. Organoids generated  
48 under alveolar differentiation conditions were cystic-like and lacked robust alveolar  
49 mature cell types. Compared with unaffected postnatal lung, congenital lung lesions  
50 were marked by clusters of EpCAM<sup>+</sup>CD73<sup>+</sup> cells in airway and cystic distal lung  
51 structures lined by simple epithelium of composed of EpCAM<sup>+</sup>SCGB1A1<sup>+</sup> cells and  
52 hyperplastic EpCAM<sup>+</sup>proSPC<sup>+</sup> cells. In non-small cell lung cancer (NSCLC), there was a  
53 marked increase in EpCAM<sup>+</sup>CD73<sup>+</sup> tumor cells enriched in inhibitory immune checkpoint  
54 molecules CD47 and programmed death-ligand 1 (PD-L1), which was associated with  
55 poor survival in lung adenocarcinoma. In conclusion, EpCAM<sup>+</sup>CD73<sup>+</sup> cells are a rare  
56 novel epithelial progenitor cell in human lung. Importantly, re-emergence of CD73 in lung  
57 adenocarcinoma enriched in negative immune checkpoint molecules may serve as a  
58 novel therapeutic target.

59 Keywords: EpCAM; congenital lung lesions; organoids; CD73; immune checkpoint;  
60 adenocarcinoma

## 61 **Introduction**

62 Despite being a quiescent organ at homeostasis, clinically the human lung does possess  
63 an ability for repair after various insults, although inherently low (5, 45). Nonetheless, the  
64 cellular and molecular mechanisms governing the regenerative process following lung  
65 injury have been slow in forthcoming. Moreover, the idea of a resident cell type within  
66 human lung with facultative stem cell function that is induced following injury remains  
67 controversial (25). Identifying putative cell populations in the human adult lung with  
68 facultative function and whether certain disease settings affect their numbers and  
69 function, may uncover new targets for therapeutic treatment to restore normal lung  
70 structure and function following various injuries.

71 In human lung, epithelial cell adhesion molecule (EpCAM/CD326) is used as a  
72 biomarker enriching a population of cells endowed with stem/progenitor-like function (2).  
73 This type I single span transmembrane glycoprotein was first described as a cell surface  
74 antigen on human carcinoma cells of epithelial origin (17). Since then, a growing body of  
75 evidence has shown that EpCAM is expressed on a dynamic range of cells and is  
76 critically involved in ensuring proper endodermal/epithelial morphogenesis (46). During  
77 development, EpCAM expression wanes in terminally differentiated cells and re-  
78 emerges during tissue regeneration and malignancy (34). Recently, a rare population of  
79 EpCAM-positive cells enriched in ecto-5'-nucleotidase/CD73 in human breast tissue was  
80 shown to possess enhanced cell plasticity giving rise to tissue from all three germ layers  
81 (38). Following this, high-dimensional analysis of single cells during cellular  
82 reprogramming revealed that  $CD73^{high}Ki67^{High}$  distinguishes partially reprogrammed  
83 cells that were  $Oct4^{high}Klf4^{high}EpCAM^{low}$  (52). This transitional cell state was found to  
84 precede mesenchymal-to-epithelial transition and then pluripotency (52). CD73 is a cell

85 surface ectoenzyme that hydrolyzes the conversion of extracellular adenosine  
86 monophosphate to adenosine (33). In the human lung, CD73 is expressed by a wide  
87 number of cells within the mesenchymal and immune compartments (33). Within the  
88 epithelial compartment, CD73 is locally expressed on the airway mucosal and serosal  
89 surface where it is functionally active in the conversion of extracellular ATP to adenosine  
90 under normal physiological conditions (37). Hypoxia results in upregulation in  
91 CD73/adenosine, which under chronic conditions becomes maladaptive (3).  
92 Overexpression of cell surface CD73 is associated with worse clinical outcome linked  
93 with excess adenosine production in both breast (4) and ovarian cancer (47). Whether  
94 CD73 can be used to identify a discrete population of EpCAM<sup>+</sup> cells with progenitor-like  
95 function in human lung is currently not known. Furthermore, the functional significance of  
96 this population in various settings of lung injury remain unexplored.

97         Here, using a multiparametric approach we demonstrate that EpCAM<sup>+</sup>CD73<sup>+</sup> cells  
98 represent a rare but stable progenitor-like population in human lung. EpCAM<sup>+</sup>CD73<sup>+</sup> are  
99 positioned along the basal membrane of respiratory epithelium, as well as in the alveolar  
100 region in unaffected postnatal human lung. Single EpCAM<sup>+</sup>CD73<sup>+</sup> cells give rise to  
101 pseudostratified epithelium in two-dimensional air-liquid interface or in a clonal 3D  
102 organoid assay, whereas under alveolar differentiation conditions clonal organoids were  
103 more cystic-like and lacked robust alveolar mature cell types. Analysis of congenital lung  
104 lesions revealed the presence of clusters of EpCAM<sup>+</sup>CD73<sup>+</sup> cells in the airway, whereas  
105 cystic distal lung structures were lined by simple epithelium consisting of  
106 EpCAM<sup>+</sup>SCGB1A1<sup>+</sup> cells and hyperplastic EpCAM<sup>+</sup>proSPC<sup>+</sup> cells. An upregulation of  
107 EpCAM<sup>+</sup>CD73<sup>+</sup> tumor cells enriched in inhibitory immune checkpoint molecules CD47

108 and programmed death-ligand 1 (PD-L1), which was associated with poor survival, was  
109 revealed in lung adenocarcinoma.

110

111 **Materials and Methods**

112 **Collection of lung tissue**

113 Collection and processing of human lung tissue was performed as previously described  
114 (49). Briefly, resected tissues were collected from pediatric patients undergoing elective  
115 surgery for congenital lung lesions and other lung abnormalities at Children's University  
116 Hospital of Zurich (see Table S1), as well as adult patients undergoing resection for non-  
117 small cell lung cancer (NSCLC) or metastasis to the lung (see Table S2 and S3) at Bern  
118 University Hospital, Department of Thoracic Surgery. The use of surgically resected  
119 material for research purposes was provided by all patients included in this study, which  
120 was approved by the Ethics Commission of the Canton of Bern (KEK-BE:042/2015). All  
121 supplemental material is available at <https://doi.org/10.6084/m9.figshare.12488867>.

122  
123 **Flow cytometric analysis, prospective cell isolation and generation of primary**  
124 **cultures**

125 Generation of single cell suspensions for flow cytometric analysis and prospective cell  
126 isolation were performed as previously described (49). Briefly, single cells from digested  
127 lung tissue were stained with fluorescently conjugated human monoclonal antibodies  
128 targeting: CD45, CD14, CD31, CD73, CD90, EpCAM (see Table S7). Following sorting,  
129 EpCAM<sup>+</sup>CD73<sup>+</sup> cells (see Figure 1C and Supplemental Fig. S1 for full gating strategy)  
130 were plated on dishes pre-coated with a solution consisting of 0.2% gelatin, 0.3 mg/ml of  
131 human collagen I (Sigma) and 0.03 mg/ml of human collagen IV (Sigma). Cells were  
132 grown in cell expansion media (see Table S8) and maintained in a humidified 37°C low  
133 oxygen (3% O<sub>2</sub>) incubator in 5% CO<sub>2</sub>. An additional FACS analysis was performed on a  
134 second cohort of postnatal (n = 6; PL017-PL022) and adult lungs (n = 6; patient 10-15,

135 see Table S1) using the same antibody backbone as described above with addition of  
136 the following antibodies: CD146, NOTCH3 and integrin  $\beta$ 4 (CD104) (see Table S7). To  
137 further immunophenotype the epithelial progenitor cell population, we stained a third  
138 cohort of lung tissue (postnatal, n = 6; PL029-PL035 and adult lungs, n = 7; patient, see  
139 Table S1 and S2) using our original antibody backbone with addition of the following  
140 antibodies: HTII-280, CD24 and PDPN (see Table S7).

141

### 142 **Immunophenotype of cell subsets using flow cytometry**

143 Following isolation and expansion of EpCAM<sup>+</sup>CD73<sup>+</sup> cells (see Figure 2A and Table  
144 S10), cells were harvested and re-suspended in FACS staining buffer. Following Fc  
145 block, cells were incubated with the following fluorescently conjugated human  
146 monoclonal antibodies: integrin  $\beta$ 4, EpCAM, CD47 (see Table S7). Cells were incubated  
147 on ice in the dark for 30 minutes. To exclude dead cells and debris, 7-AAD was added.  
148 Cell acquisition was performed using a BD FACS LSRII. For analysis, a minimum of  
149 10,000 events were collected and analyzed using FlowJo software version 10.7 (Tree  
150 Star).

151

### 152 **Immunofluorescence analysis**

153 Preparation of lung tissue for immunostaining was performed as previously described  
154 (49). Briefly, 5  $\mu$ m sections of were stained with hematoxylin & eosin using standard  
155 protocols. For immunofluorescence, 5  $\mu$ m sections were stained with a panel of human  
156 monoclonal antibodies: EpCAM, CD73, CD90, SOX2, KRT5, TRP63, integrin  $\beta$ 4,  
157 SCGB1A1 and proSPC on different tissue samples (see Table S1 and Table S8-9).  
158 Following immunostaining, high resolution images were acquired with a Zeiss LSM 710

159 Confocal Microscope. Collected images were imported into Imaris software Ver 7.6  
160 (Bitplane, CH). Quantification of cell phenotype was performed by sampling five random  
161 fields (20X) taken from disease regions and the matched normal region in three patients.  
162 Firstly, 100-200 airway epithelial cells were counted based on DAPI/EpCAM staining.  
163 Cells that were SCGB1A1<sup>+</sup> were also counted. From the same patients, the percentage  
164 of EpCAM<sup>+</sup>proSPC<sup>+</sup> cells relative to EpCAM<sup>+</sup> cells were assessed from five random  
165 fields in each slide (20X).

166

## 167 **2D air-liquid interface**

168 Passage 3 EpCAM<sup>+</sup>CD73<sup>+</sup> epithelial cells were counted and single cells were seeded  
169 onto transwell inserts (0.4 µm Transwell insert, Corning) in expansion media on both the  
170 apical and basal side of the insert. After two days, media was removed from both the  
171 apical and basal surface and cells were grown at air-liquid interface (ALI) in airway  
172 differentiation media (PneumoCult™-ALI medium, StemCell Technologies). Regular  
173 media changes from the basal surface were made every three days. After 21 days, cells  
174 were fixed with 70% ethanol (Sigma). For immunofluorescence (IF), inserts were  
175 incubated with cooled solution of 95% ethanol / 5% glacial acetic acid for 10 minutes for  
176 permeabilization and washed 3X in TBS solution. Afterwards, inserts were blocked with  
177 3% goat serum (blocking solution) for 1 hour at room temperature. Inserts were  
178 incubated overnight at 4°C with primary antibodies to detect mucous secreting cells,  
179 goblet, club and basal stem cells (see Table S6). Secondary antibodies (see Table S9)  
180 were diluted in washing solution and added to the inserts, which were incubated for 2  
181 hours at room temperature. Nuclei were counterstained with DAPI. High resolution Z-  
182 axis images were acquired with a Zeiss LSM 710 Confocal Microscope. Images were



183 collected and imported into Imaris software Ver 7.6 (Bitplane, CH) to recreate three-  
184 dimensional (3D) volume reconstruction of the data set to visualize cell surface areas  
185 and volume performed using the Surpass tool. To examine the role of the NOTCH  
186 signaling pathway, separate wells were treated with delta-like ligand 4 (DLL4, 10 ng/ml,  
187 Peprotech) or  $\gamma$ -secretase inhibitor DAPT (20  $\mu$ M, Sigma) or vehicle (DMSO, Sigma) at  
188 every media change and samples were processed for IF, as described above. From  
189 images, 5 random fields were counted in three technical replicates at 40X magnification.  
190 The total cell amounts based on the E-cadherin staining, then counted SCGB1A1<sup>+</sup>,  
191 MUC5AC<sup>+</sup> and  $\beta$ -tubulin<sup>+</sup> cells respectively.

192

### 193 **3D organoid culture**

194 To generate airway organoids, single EpCAM<sup>+</sup>CD73<sup>+</sup> cells from postnatal or adult lung  
195 were mixed with autologous CD90<sup>+</sup> stromal cells at a 1:1 ratio and resuspended in 50%  
196 solution of growth factor reduced matrigel (Corning) and seeded into inserts (0.4  $\mu$ m  
197 Transwell insert, Corning). After solidification of matrigel:cell solution, airway  
198 differentiation media (PneumoCult<sup>TM</sup>) was added to the basal chamber. Fresh media  
199 changes were made every 2 days for 21 days. To generate alveolar organoids, a 40%  
200 solution of growth factor reduced matrigel (Corning) was seeded into 0.4  $\mu$ m Transwell  
201 inserts (Corning) and allowed to solidify forming a base. Afterwards, a 5% matrigel  
202 solution containing EpCAM<sup>+</sup>CD73<sup>+</sup> cells with autologous CD90<sup>+</sup> stromal cells at a 1:1  
203 ratio was seeded onto the top of matrigel base. 800  $\mu$ l of expansion media was added to  
204 the basal chamber exposing cells to ALI. Transwell inserts were maintained in a  
205 humidified 37°C oxygen (21%) incubator in 5% CO<sub>2</sub> for expansion/differentiation. After  
206 24 hours, media was removed from the apical surface and not replaced to mimic ALI,

207 whereas a fresh media change to the lower chamber was made using distal airway  
208 media (see Table S12) and media was changed every two days. After 21 days, inserts  
209 were fixed with 70% ethanol and processed for IF or removed from matrigel using  
210 dispase (Corning). High resolution Z-axis images were acquired with a Zeiss LSM 710  
211 Confocal Microscope. Images were collected as lsm files and imported into Imaris  
212 software (Ver7.6) to recreate 3D volume reconstruction of the data set to visualize cell  
213 surface areas, organoid volume and cell-cell communication using the Surpass tool.

214

### 215 **Transmission electron microscopy**

216 Airway organoids were recovered from the matrigel using dispase (Corning) and  
217 submerged with fixative consisting of 2.5% glutaraldehyde (Agar Scientific, Stansted,  
218 Essex, UK) in 0.15M HEPES (Fluka, Buchs, Switzerland) with an osmolarity of 709  
219 mOsm and adjusted to a pH of 7.34. The organoids remained in the fixative at 4°C for at  
220 least 24h, before being further processed. All samples were then washed with 0.15 M  
221 HEPES three times for 5 min, post fixed with 1% OsO<sub>4</sub> (SPI Supplies, West Chester,  
222 USA) in 0.1 M Na-cacodylate-buffer (Merck, Darmstadt, Germany) at 4°C for 1 h,  
223 washed with 0.05 M maleat-NaOH buffer (Merck, Darmstadt, Germany) three times for 5  
224 min, and then block stained in 0.5% uranyl acetate (Fluka, Buchs, Switzerland) in 0.05 M  
225 maleat-NaOH buffer at 4°C for 1 h. Thereafter, cells were washed in 0.05 M maleat-  
226 NaOH buffer three times for 5 min and dehydrated in 70, 80 and 96% ethanol  
227 (Alcosuisse, Switzerland) for 15 min each at room temperature. Subsequently, cells  
228 were immersed in 100% ethanol (Merck, Darmstadt, Germany) three times for 10 min, in  
229 acetone (Merck, Darmstadt, Germany) two times for 10 min, and finally in acetone-epon  
230 (1:1) overnight at room temperature. The next day, cells were embedded in epon (Fluka,

231 Buchs, Switzerland) and left to harden at 60°C for 5 days. Sections were produced with  
232 an ultramicrotome UC6 (Leica Microsystems, Vienna, Austria), first semi-thin sections (1  
233 um) for light microscopy which were stained with a solution of 0.5% toluidine blue O  
234 (Merck, Darmstadt, Germany) and then ultrathin sections (70-80 nm) for electron  
235 microscopy. The sections, mounted on single slot copper grids, were stained with uranyl  
236 acetate and lead citrate with an ultrastainer (Leica Microsystems, Vienna, Austria).  
237 Sections were then examined with a transmission electron microscope (CM12, Philips,  
238 Eindhoven) equipped with a digital camera (Morada, Soft Imaging System, Münster,  
239 Germany) and image analysis software (iTEM).

240

#### 241 **RNA extraction and real time quantitative PCR**

242 Total RNA was extracted from cells or organoids using RNeasy Mini Kit (Qiagen) to  
243 analyze gene expression using real time quantitative PCR (RT-qPCR). RT-qPCR was  
244 performed in triplicates with target-specific primers using TaqMan Gene Expression  
245 Assay (Applied Biosystems) on AB7500 FAST real-time PCR system (Applied  
246 Biosystems). Expression levels were normalized to 3 internal controls tested for  
247 expression stability across samples in each experiment using Expression Suite Software  
248 (Life Technologies). Relative expression was calculated by  $2^{-\Delta\Delta CT}$  method. (see Table S6  
249 for primer list).

250

#### 251 **PD-L1 and CD47 immunohistochemistry**

252 Serial sections from formalin-fixed and paraffin-embedded human lung adenocarcinoma  
253 (LUAD, n = 27) and lung squamous cell carcinoma (LUSC, n = 31) cases were stained  
254 for programmed death ligand-1 (PD-L1) and CD47. Immunohistochemical staining was

255 performed using an automated immunostainer (Bond III, Leica Biosystems, MuttENZ,  
256 Switzerland) using the following antibodies: anti-human PD-L1 (clone E1L3N, Cell  
257 Signaling Technology, Damvers, MA, USA) at a dilution of 1:400 and anti-human CD47  
258 (clone B6H12, Santa Cruz, San Diego, USA) at a dilution of 1:20. Sections were  
259 incubated with primary antibodies at room temperature for 15 minutes, followed by  
260 incubation with the secondary antibody using the Bond Polymer Refine Kit with 3-3'-  
261 Diaminobenzidine-DAB as chromogen (Leica Biosystems), counterstained with  
262 hematoxylin and mounted in Aquatex (Merck, Darmstadt, Germany). Membranous CD47  
263 expression was scored 0-3 by a trained pathologist (SB). Tumoral PD-L1 expression  
264 was scored by a trained pathologist (SB) according to current guidelines as the  
265 percentage of cells with membranous staining of any intensity (tumor proportion score)  
266 and grouped as follows: <1%; between 1 to <50%; and  $\geq$ 50%, as previously described  
267 (22) (see Table S5 and S6). For double immunohistochemistry of postnatal lung tissue,  
268 rabbit PD-L1 antibody (clone E1L3N) was diluted 1:400, incubated for 30 min. Samples  
269 were incubated with Horseradish Peroxidase (HRP)-polymer for 15 min and visualized  
270 using DAB as brown chromogen (Bond polymer refine detection, Leica Biosystems) for  
271 10 min. Following this, slides were incubated with mouse ERG antibody (Agilent,  
272 M73149) diluted at 1:50 for 30 min. Following this, slides were incubated with secondary  
273 antibody Alkaline phosphatase (AP)-polymer for 15 min, and visualized using fast red as  
274 red chromogen (Red polymer refine Detection, Leica Biosystems). Samples were  
275 counterstained with haematoxylin and mounted with Aquatex (Merck). All slides were  
276 scanned and photographed using Panoramic 250 (3DHistech).

277

## 278 **Statistical analysis**

279 Data are expressed as mean  $\pm$  SD. Comparisons between two groups were carried out  
280 using the parametric student's two-tailed paired or unpaired t-test for normally distributed  
281 data. If data were not distributed normally, a nonparametric Wilcoxon signed-rank test  
282 was used between the two groups. All tests were two-tailed. Analysis of more than two  
283 groups was performed with ANOVA followed by Newman-Keuls post hoc test. The  
284 numbers of samples (biological replicates) per group (n), or the numbers of experiments  
285 (technical replicates) are specified in the figure legends. Data was analyzed using  
286 GraphPad Prism 8 software. Statistical significance is accepted at  $P < 0.05$ .

287 **Results**

288 **CD73<sup>+</sup> labels a rare population of EpCAM<sup>+</sup> progenitor cells in both airway and**  
289 **alveolar region of unaffected human lung**

290 As shown in the schematic panel in Figure 1A, we applied a multiparametric approach to  
291 identify and characterize resident lung epithelial progenitor cells in a cohort of pediatric  
292 patients (herein called postnatal) undergoing elective surgery for congenital lung lesions  
293 and other airway abnormalities (see Table S1) and adult patients diagnosed with  
294 NSCLC undergoing elective surgery for curative intent (see Table S3). We previously  
295 reported the presence of an EpCAM<sup>neg</sup> (gate R4) mesenchymal cluster further  
296 fractionated on the basis of CD73/CD90 in unaffected postnatal lung using  
297 polychromatic flow cytometry (49). Here, unlike cells in the EpCAM<sup>neg</sup>, we show that the  
298 EpCAM<sup>pos</sup> fraction (gate R5, Figure 1B and Fig. S1A) contains a cluster of cells enriched  
299 for 5`ecto-nucleotidase CD73 (gate R6, 11.8±9.9%, Figure 1C and Supplemental Fig.  
300 S1A, D). In contrast, CD73<sup>+</sup> cells co-expressing membrane glycoprotein CD90 (THY-1)  
301 or single CD90<sup>+</sup> cells were rare (CD73<sup>+</sup>CD90<sup>+</sup>, 0.8±0.8% and CD73<sup>-</sup>CD90<sup>+</sup>, 3.9±2.8%,  
302 Figure 1D and Supplemental Fig. S1B-E). Surprisingly, there was no difference in the  
303 percent of EpCAM<sup>+</sup>CD73<sup>+</sup> cells between postnatal and adult lung tissue (Figure 1E and  
304 Supplemental Fig. S1F).

305 Next, we wanted to localize EpCAM<sup>+</sup>CD73<sup>+</sup> cells in postnatal lung. Apart from  
306 standard histological analysis based on H&E performed on unaffected lung tissue  
307 (Figure 1F-H), we immunostained separate sections with EpCAM and CD73. Confocal  
308 analysis revealed dual EpCAM/CD73 labelled cells occupying a basal position in the  
309 airway (Figure 1G, white arrow). In the alveolar region, cuboidal shaped cells co-staining  
310 for EpCAM and CD73 (white arrows) were found next to flat squamous-like CD73<sup>+</sup> cells

311 (white arrowhead) lacking EpCAM (Figure 1I). Further, EpCAM<sup>+</sup> cells in the airway co-  
312 stain with the transcription factor SRY-Box 2 (SOX2), whereas in the alveolar region  
313 were shown to express the AII marker prosurfactant protein C (proSPC) (Supplemental  
314 Fig. S1G-H).

315  
316 **Prospectively isolated EpCAM<sup>+</sup>CD73<sup>+</sup> cells resemble basal-like stem cells in**  
317 **culture**

318 Next, using FACS we prospectively isolated EpCAM<sup>+</sup>CD73<sup>+</sup> cells from unaffected  
319 postnatal lung tissue and expanded cells in feeder-free plates using a chemically-  
320 defined growth media (Figure 2A). At the mRNA level, EpCAM<sup>+</sup>CD73<sup>+</sup> cells were  
321 enriched for SOX2 and Keratin 5 (KRT5), as well as the basal stem cell transcription  
322 factor p63 (TRP63) (Figure 2B). Expression of genes defining mature cell types were not  
323 observed or low. Interestingly, there was a 2-fold increase in hypoxia inducible factor  
324 HIF1 $\alpha$  expression in EpCAM<sup>+</sup>CD73<sup>+</sup> cells (Figure 2B). Immunostaining sorted cells after  
325 reaching confluence in culture revealed that the majority of expanded EpCAM<sup>+</sup>CD73<sup>+</sup>  
326 cells express the laminin receptor integrin  $\beta$ 4, which supports cell adhesion between  
327 basal epithelial cells and basement membrane (28). This was confirmed using flow  
328 cytometry (Supplemental Fig. S2A). Variable expression for SOX2 and KRT5 were  
329 observed, as well as lack of expression of proSPC and the club cell marker SCGB1A1  
330 (Figure 2C-E). FACS analysis on independent postnatal specimens revealed that a  
331 small fraction of postnatal EpCAM<sup>+</sup>CD73<sup>+</sup> cells co-express integrin  $\beta$ 4 *ex vivo*  
332 (Supplemental Fig. S2B), which did not differ in adult lung (postnatal, 10.7 $\pm$ 11% versus  
333 adult, 7.1 $\pm$ 5.6%, Supplemental Fig. S2C). Immunostaining of postnatal human lung  
334 revealed integrin  $\beta$ 4<sup>+</sup> cells located along the basal membrane of the conducting airway

335 co-expressing KRT5 (Supplemental Fig. S2D), whereas integrin  $\beta 4^+$  cells co-expressing  
336 proSPC in the alveolar region were rare (Supplemental Fig. S2E-F). To further  
337 immunophenotype the EpCAM<sup>+</sup>CD73<sup>+</sup> population *in vivo*, we stained an additional six  
338 independent postnatal and seven adult tissue samples and show that a small subset  
339 within the EpCAM<sup>+</sup>CD73<sup>+</sup> population co-express the ATII marker HTII-280 (15) in both  
340 postnatal (3.6±2.5%) and adult human lung (3.4±4.2%) (Figure 2F-G and Supplemental  
341 Fig. S2G, H). Moreover, sequential gating show variable expression of CD24 and PDPN  
342 within EpCAM<sup>+</sup>CD73<sup>+</sup>HTII-280<sup>-</sup> and EpCAM<sup>+</sup>CD73<sup>+</sup>HTII-280<sup>+</sup> subsets (Supplemental  
343 Fig. S2I-K). Taken together, EpCAM<sup>+</sup>CD73<sup>+</sup> cells represent a rare but heterogeneous  
344 population in human lung. Our submersion culture conditions appear to favour the  
345 expansion of cells toward a SOX2<sup>+</sup> basal stem-cell like state (Figure 2H), consistent with  
346 primary sorted Sox2<sup>+</sup>EpCAM<sup>+</sup> $\beta 4^+$ Krt5<sup>-</sup> progenitor cells derived from murine lungs (50).

347

### 348 **Generating airway epithelium from single EpCAM<sup>+</sup>CD73<sup>+</sup> cells**

349 Based on the location of EpCAM<sup>+</sup>CD73<sup>+</sup> cells in the airway of postnatal lung and gene  
350 expression pattern following expansion in culture, we next investigated the airway  
351 differentiation capability of EpCAM<sup>+</sup>CD73<sup>+</sup> cells from postnatal and adult lung tissue.  
352 Standard H&E of a lung section from the unaffected postnatal lung show normal lung  
353 structure including a bronchiole and surrounding alveolus (Figure 3A and Supplemental  
354 Fig. S3A). Using confocal microscopy, a single bronchiole is highlighted showing the  
355 airway epithelium stains for EpCAM/SOX2, whereas KRT5<sup>+</sup> cells (green) can be seen  
356 occupying the basal layer only (Figure 3B and Supplemental Fig. S3B). In separate  
357 sections, epithelial cells lining the basal membrane of the airway express the basal stem  
358 cell marker TRP63 (white arrowhead), some of which co-express KRT5 (white arrow,



359 Figure 3C and Supplemental Fig. S3C). We seeded single FACS-sorted EpCAM<sup>+</sup>CD73<sup>+</sup>  
360 cells at air-liquid-interface (ALI) to induce airway differentiation (Figure 3D). After 21  
361 days, postnatal EpCAM<sup>+</sup>CD73<sup>+</sup> cells give rise to pseudostratified multiciliated-secretory  
362 epithelium (left panels, Figure 3D and Supplemental video S1). Persistent  
363 pharmacological activation of NOTCH signaling using the precanonical NOTCH ligand  
364 DLL4 during airway differentiation reduced both goblet (MUC5AC, white) and secretory  
365 club cell (SCGB1A1, purple) formation whereas cilia ( $\beta$ -tubulin, yellow) formation was  
366 intact (middle panels, Figure 3D and Supplemental Fig. S3D). Immunostaining with E-  
367 cadherin (green) and 3D volume rendering through the zy plane show an intact  
368 pseudostratified barrier and TRP63<sup>+</sup> (red) cells along the basal membrane (Figure 3D-  
369 E). Pharmacological inhibition of NOTCH signaling using gamma secretase inhibitor  
370 DAPT also decreased the formation of both goblet cells and secretory club cells leaving  
371 cilia formation intact (far right panels, Figure 3D and Supplemental Fig. S3D). However,  
372 formation of a pseudostratified barrier was disrupted (Figure 3E). In comparison with  
373 adult-derived EpCAM<sup>+</sup>CD73<sup>+</sup> cells, we noted several differences (Figure 3F). First, adult-  
374 derived EpCAM<sup>+</sup>CD73<sup>+</sup> cells required the presence of autologous CD90<sup>+</sup> stromal cells to  
375 ensure proper airway differentiation (left panels, Figure 3F and Supplemental video S2).  
376 Second, the formation of a mucociliary epithelium was intact despite persistent NOTCH  
377 signaling (middle panels Figure 3F and Supplemental Fig. S3E). Third, inhibition of  
378 NOTCH signaling reduced cilia formation (Figure 3F and Supplemental Fig. S3E), yet  
379 the disruption in the formation of pseudostratified barrier was similar with postnatal lung  
380 EpCAM<sup>+</sup>CD73<sup>+</sup> cells (Figure 3G).

381

382 **EpCAM<sup>+</sup>CD73<sup>+</sup> cells generate three-dimensional organoid structures with airway**  
383 **and alveolar-like features**

384 The self-organizing feature possessed by adult stem cells is indispensable for the  
385 formation of organoids, which are three dimensional (3D) structures recapitulating  
386 important characteristics of the organ they represent (32). Thus, we next asked whether  
387 EpCAM<sup>+</sup>CD73<sup>+</sup> cells could give rise to organoids that recapitulate human airway found  
388 *in vivo*. We seeded single EpCAM<sup>+</sup>CD73<sup>+</sup> cells together with single autologous CD90<sup>+</sup>  
389 mesenchymal cells from the postnatal or adult lung in 3D matrigel, exposing the apical  
390 surface to air while culturing in human airway differentiation media in the basal chamber  
391 (Figure 4A). After 21 days, transmission electron microscopy demonstrated that  
392 organoid structures were morphologically similar to *in vivo* pseudostratified mucociliary  
393 epithelium (Figure 4B). Ciliated cells and secretory cells can be found facing inside the  
394 lumen of the organoid structure and small basal-like cells in the basal layer. At the  
395 mRNA level, airway organoid structures upregulated genes found to be enriched in  
396 airway (Figure 4C). Organoids with beating cilia can be detected after removal from  
397 matrigel (Supplemental video 3 and 4).

398 Next, we explored whether EpCAM<sup>+</sup>CD73<sup>+</sup> cells could generate organoids with  
399 alveolar-like features. Single postnatal EpCAM<sup>+</sup>CD73<sup>+</sup> cells with autologous CD90<sup>+</sup>  
400 stromal cells were suspended in a solution of matrigel (5%), which was overlaid on a  
401 base of matrigel (40%) and grown in a modified alveolar induction media placed in the  
402 basal chamber biased towards alveolar differentiation (Figure 4D). After 21 days,  
403 confocal imaging of an organoid shows the presence of rare ATII-like cells positive for  
404 proSPC at the apical surface of the lumen (white arrow, Figure 4E and Supplemental  
405 Fig. S4A-B). In separate organoids, rare cells positive for the ATI marker HOPX can be

406 observed, which were distinct from KRT5<sup>+</sup> stained cells (Figure 4F and Supplemental  
407 Fig. S4C). Similar results were observed for alveolar organoids derived from adult  
408 EpCAM<sup>+</sup>CD73<sup>+</sup> cells (Supplementary Fig. S4D-E). FACS analysis revealed the presence  
409 of EpCAM<sup>+</sup>CD73<sup>+</sup>HTII-280<sup>-</sup> and EpCAM<sup>+</sup>CD73<sup>+</sup>HTII-280<sup>+</sup> cells using FACS at levels  
410 similar to those found *in vivo* (Figure 4G, H). However, the level of single positive HTII-  
411 280 epithelial cells was diminished (organoids, 13.42±4.84% and postnatal lung,  
412 55.3±26.7%). Co-expression of CD24 and PDPN were upregulated in alveolar organoids  
413 (Figure 4I, J). Moreover, a greater percent of EpCAM<sup>+</sup>CD73<sup>+</sup> cells co-expressed β4<sup>+</sup>  
414 cells compared with *in vivo* native postnatal lung (organoids, 40.6±31% and postnatal  
415 lung, 11.55±15%) (Supplemental Fig. S4F-G).

416

417 **Expansion of EpCAM<sup>+</sup>CD73<sup>+</sup> cells together with mature epithelial cell lineages in**  
418 **congenital lung lesions and other airway abnormalities**

419 To determine whether the EpCAM<sup>+</sup>CD73<sup>+</sup> cell subset or other cell lineages are induced  
420 after lung injury, we performed immunofluorescence analysis of matched lung tissue  
421 obtained from patients diagnosed with congenital lung lesions and other airway  
422 abnormalities (Table S1). Standard H&E staining show structural airway malformations  
423 and cystic lesions from representative patients (Figure 5A-D and Supplemental Fig. S5).  
424 In highlighted regions of H&E sections (Figure 5E, G), clusters of EpCAM<sup>+</sup>CD73<sup>+</sup> cells in  
425 the airway of a patient with CPAM (Figure 5F) or chronic bronchiolitis (Figure 5H) can be  
426 observed with confocal imaging. In a separate patient with congenital intrapulmonary  
427 sequestration, H&E shows the dysplastic alveolar epithelium (Figure 5I) and  
428 corresponding confocal image shows the extent of EpCAM/CD73 localization (Figure  
429 5J). There was no evidence of clusters of TRP63<sup>+</sup>KRT5<sup>+</sup> cells migrating from the

430 proximal airway or ectopic TRP63<sup>+</sup>KRT5<sup>+</sup> or KRT5<sup>+</sup> cells in the distal lung between  
431 cystic lesions or in dysplastic alveolar regions in CPAM tissue (Figure S6D-F).  
432 Moreover, in these same patients, EpCAM<sup>+</sup>SOX2<sup>+</sup> or EpCAM<sup>+</sup>SOX2<sup>+</sup>KRT5<sup>+</sup> cells were  
433 observed in the basal layer of cysts but not in the thickened interstitium (Supplemental  
434 Fig. S6G-I).

435 Confocal imaging analysis demonstrated that cystic lesions and areas of  
436 dysplastic alveolar epithelium were lined with hyperplastic EpCAM<sup>+</sup>proSPC<sup>+</sup> cells (yellow  
437 arrow), either as single cells or as clusters in patients with congenital lung lesions  
438 (Figure 6A-F). In other regions, bronchiolar lined cysts of cuboidal and columnar  
439 epithelium stained positive for EpCAM<sup>+</sup>SCGB1A1<sup>+</sup> (yellow arrowhead), as well as lining  
440 the airways in the damaged region of the lung (Figure 6A-F). We noted a significant  
441 increase in both EpCAM<sup>+</sup>proSPC<sup>+</sup> and EpCAM<sup>+</sup>SCGB1A1<sup>+</sup> cell subtypes (Figure 6G). In  
442 cystic lung lesions we did not observe dual positive proSPC-SCGB1A1 cells indicative of  
443 putative bronchioalveolar stem/progenitor cell with regenerative potential, as described  
444 in various mouse models of lung injury (29, 40).

#### 445 446 **EpCAM<sup>+</sup>CD73<sup>+</sup> cells re-emerge in lung adenocarcinoma and upregulate immune** 447 **checkpoint molecules PD-L1 and CD47**

448 CD73 has emerged as a novel therapeutic target in solid tumors due its role in the  
449 enzymatic generation of the immunosuppressive molecule adenosine (1). We  
450 investigated whether there is re-emergence of CD73 expression on tumor epithelial cells  
451 marked by EpCAM in NSCLC and whether this cell cluster expresses additional  
452 inhibitory immune checkpoint molecules involved in immune resistance. To accomplish  
453 this, we profiled the composition of tumor epithelium (EpCAM<sup>+</sup>) and matched uninvolved

454 lung tissue using polychromatic flow cytometry in a cohort of 122 surgically resected  
455 stage I to IV NSCLC tissues. Clinical and pathologic characteristics for all patients are  
456 found in Table S3. In representative patients, H&E staining shows tumor islands  
457 surrounded by stroma (Figure 7A, C and Supplemental Fig. S7). Confocal imaging  
458 demonstrated that EpCAM<sup>+</sup> tumor islands co-stain for CD73 (Figure 7B). A serial section  
459 confirmed that these cells also were TRP63 positive (Figure 7D and Supplemental Fig.  
460 S7B-C, E). Flow cytometric analysis demonstrated an enrichment in EpCAM<sup>+</sup> tumor cells  
461 co-expressing CD73 in lung adenocarcinoma (LUAD) (Figure 7E). In the lung squamous  
462 cell carcinoma (LUSC) cohort, there was an enrichment in EpCAM<sup>+</sup>CD73<sup>+</sup> cells in tumor  
463 in subsets of patients; however, overall this was not significant (Figure 7F). The  
464 inhibitory immune checkpoint molecule PD-L1 was upregulated in the EpCAM<sup>+</sup>CD73<sup>+</sup>  
465 TC fraction in both LUAD and LUSC (Figure 7G, H). Interestingly, membrane expression  
466 of CD47, a “don’t eat me signal” and inhibitory checkpoint molecule of the innate  
467 immune system, was found to be overexpressed in the EpCAM<sup>+</sup>CD73<sup>+</sup> TC fraction only  
468 in LUAD (Figure 7G, H). Comparison of LUAD with LUSC revealed a difference only in  
469 EpCAM<sup>+</sup>CD73<sup>+</sup> cells (Supplemental Fig. S7F-I). To determine the level of colocalization  
470 of tumoral PD-L1 and CD47, we performed immunohistochemistry on serial sections of  
471 58 NSCLC cases (LUAD, n = 27; LUSC, n = 31). Representative micrographs of serial  
472 sections capture the heterogeneity in tumoral PD-L1 and CD47 co-expression (Figure  
473 7I), which was depicted in an expanded number of cases (Supplemental Fig. S7J-K) and  
474 quantified in table format (Supplemental Table S5 and S6). Surprisingly, we did not  
475 detect PD-L1 expression within the epithelium of congenital lung lesions we examined  
476 despite immune infiltration being present in some case (Supplemental Fig. S8).

477           Based on the compositional features identified in LUAD and LUSC the following 6  
478 markers CD73 (NT5E), EpCAM (EPCAM), CD90 (THY1), PD-L1 (CD274), CD47 and  
479 CD127 (IL-7R) were used to determine their clinical relevance in predicting patient  
480 survival using mRNA expression data from The Cancer Gene Atlas (TCGA) NSCLC  
481 cohort. We were able to build a compound Cox proportional-hazards model to find the  
482 best combination of the 6-gene signature associated with survival. In LUAD, we found a  
483 compound model whereby increased expression of CD73 at the mRNA level was  
484 associated with shorter patient survival, whereas this was not the case for LUSC (Figure  
485 7J). Taken together, these data highlight the importance of CD73 as a potential novel  
486 drug target in adenocarcinoma histology.

487

488 **Discussion**

489 Here, we show that CD73 enriches for a rare EpCAM<sup>+</sup> cell subset isolated from healthy  
490 postnatal and adult human lung tissue that can give rise to pseudostratified mucociliary  
491 epithelium, and to a limited extent, mature alveolar cell types. Spatially, EpCAM/CD73  
492 double positive cells were found in the respiratory epithelium and alveolar region.  
493 Importantly, this rare population remains stable during lung maturation. In congenital  
494 cystic lung lesions and other airway abnormalities foci of EpCAM<sup>+</sup>CD73<sup>+</sup> cells line the  
495 airway epithelium. Interestingly, in LUAD EpCAM<sup>+</sup>CD73<sup>+</sup> cells re-emerge and co-  
496 express CD47 and PD-L1, proteins that negatively regulate host innate and adaptive  
497 immune responses, respectively, and are known to contribute to tumor immune escape.

498 A significant challenge in the field is the use of surface-marker based phenotyping  
499 to identify cell types in human lung endowed with stem cell function under stable  
500 conditions and during perturbations. Using EpCAM as a surrogate marker of normal lung  
501 stem cells, Hogan and colleagues were the first to demonstrate that EpCAM<sup>+</sup> cells co-  
502 expressing the ATII marker HTII-280 (15) function as bona fide ATII stem cells when  
503 cocultured with niche cells (2). Following this, numerous studies have since confirmed  
504 the use of EpCAM to isolate lung progenitors from human iPSCs to generate 3D lung  
505 organoids with both airway and alveolar features (8, 12, 16), and to isolate ATII cells for  
506 downstream characterization within adult human lung (7, 9) Using a flow cytometric  
507 approach, we demonstrate that a small subset of postnatal lung EpCAM<sup>+</sup>CD73<sup>+</sup> cells co-  
508 express this HTII-280, which does not change with age. The alveolar differentiation  
509 potential of EpCAM<sup>+</sup>CD73<sup>+</sup> cells was rare, despite immunostaining data showing  
510 anatomically distinct cuboidal shaped EpCAM<sup>+</sup>CD73<sup>+</sup> cells in the alveolar region. In  
511 sharp contrast, 2D or 3D airway differentiation potential of culture expanded

512 EpCAM<sup>+</sup>CD73<sup>+</sup> cells was robust. A limitation may be the inability to expand bona fide  
513 human alveolar progenitor cells, which are SFPC<sup>+</sup> (18) and the intervening period of  
514 submersion culture *in vitro*. In murines, submersion culture induces hypoxia-driven  
515 hyperactive NOTCH signaling that favour the expansion of cells toward a Sox2<sup>+</sup> basal  
516 stem-cell like state and impairs their alveolar differentiation potential (50). We observed  
517 that 11% of EpCAM<sup>+</sup>CD73<sup>+</sup> cells *in vivo* express integrin  $\beta$ 4, yet after submersion culture  
518 integrin  $\beta$ 4 was universally expressed. Therefore, 2D *in vitro* culture may select for  
519 airway-derived EpCAM<sup>+</sup>CD73<sup>+</sup> cells that are committed towards a basal cell state.  
520 Interestingly, a fraction of EpCAM<sup>+</sup>CD73<sup>+</sup>HTII-280<sup>+</sup> cells were recovered from alveolar  
521 organoids similar to what was observed in native lung. Despite this, we noted that the  
522 percent of EpCAM<sup>+</sup>HTII-280<sup>+</sup> cells was considerably lower compared with native lung.  
523 Alveolar organoids were generated with autologous CD90<sup>+</sup> mesenchymal cells in a  
524 media that has been shown to favour alveospheres (2). Whether CD90<sup>+</sup> mesenchymal  
525 cells this impairs alveolar differentiation due to excessive TGF- $\beta$ 1 activation originating  
526 from the mesenchyme compartment requires further investigation (35).

527 CPAM includes a wide range of developmental lung malformations arising *in*  
528 *utero* marked by cystic and/or adenomatous pulmonary areas, which was consistent with  
529 previous reports (14, 26, 43, 44). In between cystic airspaces, the distal lung is marked  
530 by thickened interstitial spaces lined by simple epithelium with expanding EpCAM<sup>+</sup> cells  
531 expressing the club cell marker secretoglobin SCGB1A1, whereas dysplastic alveolar  
532 epithelium is marked by cuboidal EpCAM<sup>+</sup> cells coexpressing proSPC. We did not  
533 observe SCGB1A1<sup>+</sup>proSPC<sup>+</sup> putative bronchioalveolar stem cells nor regenerating pods  
534 of TRP63<sup>+</sup>KRT5<sup>+</sup> cells, as has been described in murine models of lung injury and  
535 cancer (23, 24, 30, 39, 40, 48). Although incompletely understood, CPAM is thought to



536 arise due to altered branching morphogenesis during fetal lung development. Recent  
537 evidence based on transcriptome-wide analysis of congenital lung lesions revealed  
538 dysregulated expression of genes related to RAS and PI3K-AKT-mTOR pathway  
539 together with a cell-autonomous defect in growth and airway differentiation of isolated  
540 EpCAM<sup>+</sup> cells (44). (49). EpCAM is not restricted to the respiratory tract, however and  
541 whether these cells were enriched in CD73 and the mechanism driving their expansion  
542 was not described. In human fetal lung explants, coordination between highly  
543 proliferative dual positive SOX2-SOX9 progenitor cells located at distal branching tips  
544 with smooth muscle cells (SMC) in time and space is implicated in proper branching  
545 morphogenesis (10). Importantly, we show that EpCAM<sup>+</sup>CD73<sup>+</sup> cells co-express both  
546 SOX2 and SOX9 at the mRNA level. We previously demonstrated in CPAM that thick  
547 interstitial spaces were filled with mesenchymal cells (49). It is presently unclear whether  
548 the mesenchyme plays a causative role in congenital lung lesions and requires further  
549 investigation.

550         The natural evolution of CPAM also poses an increased risk for malignancy,  
551 although the true incidence is still not known (26). Lung tumors associated with CPAM in  
552 children range from rhabdomyosarcoma (RMS), pleuro-pulmonary blastoma (PPB),  
553 whereas in the adult, bronchioalveolar carcinoma (BAC) and adenocarcinoma are more  
554 common (6). Goblet cell proliferation, which has been described in CPAM may represent  
555 a precursor lesion to lung adenocarcinoma in children (13). Along these lines, various  
556 changes in several notable genes including FGF10, FGFR2b, SOX2 and mutations in  
557 KRAS at codon 12 was associated with adenocarcinoma. Recently, whole exome  
558 sequencing a cohort of eighteen CPAM patients revealed mutations linked to lung  
559 development and cancer development (19). As eluded to above, one of the main

560 difficulties has been in inability to identify the cell of origin of lung cancer in humans.  
561 Moving forward it will be necessary to perform single-cell transcriptome analysis and  
562 differentiation trajectory inference to uncover the fate of EpCAM<sup>+</sup>CD73<sup>+</sup> cells when  
563 moving from normal to aged and CPAM lung (51).

564         Regulatory networks important during development can re-emerge after tissue  
565 injury and malignant transformation (17). One such regulatory molecule is CD73. Our  
566 data in LUAD along with findings from breast (4) and ovarian cancer (47) suggest that  
567 CD73 represents a critical target in solid tumors. Functionally, this cell type ectoenzyme  
568 CD73 involved in generation of the signaling molecule adenosine via dephosphorylation  
569 of adenosine monophosphate. Production of extracellular adenosine functions as an  
570 immune suppressor initiating a cascade of events that counterbalance pro-inflammation.  
571 Under chronic inflammatory conditions, adenosine signalling can be maladaptive  
572 contributing to tumor immune escape (42). Although we did not correlate the increased  
573 tumoral CD73 expression with tumor genotype, Nakagawa and colleagues reported  
574 CD73 expression on tumor cells in *EGFR*-mutation positive NSCLC increased after  
575 targeted treatment in patients with previously high PD-L1 expression (21). In triple  
576 negative breast cancer, chemotherapy enriches for a subset of tumor cells co-  
577 expressing CD73/CD47/PD-L1 with immune evasive properties regulated, in part, via  
578 HIF1 $\alpha$  (41). A limitation in our study is that we did not correlate increased membrane  
579 expression with enzymatic activity and extracellular adenosine production. In NSCLC,  
580 immune checkpoint inhibitors targeting PD-L1/PD-1 axis have shown clinically  
581 meaningful response rates in approximately 20% of patients; however, the majority of  
582 patients still derive no therapeutic benefit from immune checkpoint blockade (11).  
583 Recently, dual targeting of CD47 and PD-L1 on tumor cells in immunocompetent

584 preclinical mouse models showed enhanced therapeutic efficacy in controlling tumor  
585 growth, in part, via re-invigoration of the host immune system (27, 31). Therefore,  
586 targeting CD73 in combination with immune checkpoint blockers targeting PD-L1 and  
587 CD47 might represent a novel treatment strategy in a subset of patients with LUAD (20,  
588 36) that requires further investigation.

589

590 **ACKNOWLEDGEMENTS**

591 Tissue were provided by the Tissue Bank Bern. Electron microscopy sample preparation  
592 and imaging were performed with devices supported by the Microscopy Imaging Center  
593 (MIC) of the University of Bern. We thank Barbara Krieger from the Institute of Anatomy,  
594 University of Bern for preparation of the EM figures. We thank staff from the FACSLab  
595 Core facility, Department of BioMedical Research, University of Bern for their assistance  
596 in performing the sorting experiments.

597  
598 **AUTHOR CONTRIBUTIONS:** conception & design – LW, SRRH; Data acquisition – LW,  
599 PD, CS, LF, SB, STS, BH, FB, CW, RWP, TMM, PKB, UM, RAS, SRRH; Data  
600 interpretation & analysis – LW, PD, SB, STS, PKB, UM, SRRH; Drafting of Manuscript –  
601 LW, SRRH; Editing of manuscript - Final Approval of manuscript – LW, RAS, SRRH.

602

603

604 **References**

- 605 1. **Antonioli L, Yegutkin GG, Pacher P, Blandizzi C, and Hasko G.** Anti-CD73 in  
606 cancer immunotherapy: awakening new opportunities. *Trends in cancer* 2: 95-109, 2016.
- 607 2. **Barkauskas CE, Crouce MJ, Rackley CR, Bowie EJ, Keene DR, Stripp BR,**  
608 **Randell SH, Noble PW, and Hogan BL.** Type 2 alveolar cells are stem cells in adult  
609 lung. *The Journal of clinical investigation* 123: 3025-3036, 2013.
- 610 3. **Borea PA, Gessi S, Merighi S, Vincenzi F, and Varani K.** Pathological  
611 overproduction: the bad side of adenosine. *British journal of pharmacology* 174: 1945-  
612 1960, 2017.
- 613 4. **Buisseret L, Pommey S, Allard B, Garaud S, Bergeron M, Cousineau I,**  
614 **Ameys L, Bareche Y, Paesmans M, Crown JPA, Di Leo A, Loi S, Piccart-Gebhart M,**  
615 **Willard-Gallo K, Sotiriou C, and Stagg J.** Clinical significance of CD73 in triple-  
616 negative breast cancer: multiplex analysis of a phase III clinical trial. *Annals of oncology*  
617 *: official journal of the European Society for Medical Oncology* 29: 1056-1062, 2018.
- 618 5. **Butler JP, Loring SH, Patz S, Tsuda A, Yablonskiy DA, and Mentzer SJ.**  
619 Evidence for adult lung growth in humans. *The New England journal of medicine* 367:  
620 244-247, 2012.
- 621 6. **Casagrande A, and Pederiva F.** Association between Congenital Lung  
622 Malformations and Lung Tumors in Children and Adults: A Systematic Review. *Journal*  
623 *of thoracic oncology : official publication of the International Association for the Study of*  
624 *Lung Cancer* 11: 1837-1845, 2016.
- 625 7. **Castaldi A, Horie M, Rieger ME, Dubourd M, Sunohara M, Pandit K, Zhou B,**  
626 **Offringa IA, Marconett CN, and Borok Z.** Genome-wide integration of microRNA and  
627 transcriptomic profiles of differentiating human alveolar epithelial cells. *American journal*  
628 *of physiology Lung cellular and molecular physiology* 2020.
- 629 8. **Chen YW, Huang SX, de Carvalho A, Ho SH, Islam MN, Volpi S, Notarangelo**  
630 **LD, Ciancanelli M, Casanova JL, Bhattacharya J, Liang AF, Palermo LM, Porotto**  
631 **M, Moscona A, and Snoeck HW.** A three-dimensional model of human lung  
632 development and disease from pluripotent stem cells. *Nature cell biology* 19: 542-549,  
633 2017.
- 634 9. **Correll KA, Edeen KE, Zemans RL, Redente EF, Serban KA, Curran-Everett**  
635 **D, Edelman BL, Mikels-Vigdal A, and Mason RJ.** Transitional human alveolar type II  
636 epithelial cells suppress extracellular matrix and growth factor gene expression in lung  
637 fibroblasts. *American journal of physiology Lung cellular and molecular physiology* 2019.
- 638 10. **Danopoulos S, Alonso I, Thornton ME, Grubbs BH, Bellusci S, Warburton D,**  
639 **and Al Alam D.** Human lung branching morphogenesis is orchestrated by the  
640 spatiotemporal distribution of ACTA2, SOX2, and SOX9. *American journal of physiology*  
641 *Lung cellular and molecular physiology* 314: L144-L149, 2018.
- 642 11. **Doroshov DB, Sanmamed MF, Hastings K, Politi K, Rimm DL, Chen L,**  
643 **Melero I, Schalper KA, and Herbst RS.** Immunotherapy in Non-Small Cell Lung  
644 Cancer: Facts and Hopes. *Clinical cancer research : an official journal of the American*  
645 *Association for Cancer Research* 2019.
- 646 12. **Dye BR, Hill DR, Ferguson MA, Tsai YH, Nagy MS, Dyal R, Wells JM,**  
647 **Mayhew CN, Nattiv R, Klein OD, White ES, Deutsch GH, and Spence JR.** In vitro  
648 generation of human pluripotent stem cell derived lung organoids. *eLife* 4: 2015.

- 649 13. **Fakler F, Aykutlu U, Brcic L, Eidenhammer S, Thueringer A, Kashofer K,**  
650 **Kulka J, Timens W, and Popper H.** Atypical goblet cell hyperplasia occurs in CPAM 1,  
651 2, and 3, and is a probable precursor lesion for childhood adenocarcinoma. *Virchows*  
652 *Archiv : an international journal of pathology* 2019.
- 653 14. **Fowler DJ, and Gould SJ.** The pathology of congenital lung lesions. *Seminars in*  
654 *pediatric surgery* 24: 176-182, 2015.
- 655 15. **Gonzalez RF, Allen L, Gonzales L, Ballard PL, and Dobbs LG.** HTII-280, a  
656 biomarker specific to the apical plasma membrane of human lung alveolar type II cells. *J*  
657 *Histochem Cytochem* 58: 891-901, 2010.
- 658 16. **Gotoh S, Ito I, Nagasaki T, Yamamoto Y, Konishi S, Korogi Y, Matsumoto H,**  
659 **Muro S, Hirai T, Funato M, Mae S, Toyoda T, Sato-Otsubo A, Ogawa S, Osafune K,**  
660 **and Mishima M.** Generation of alveolar epithelial spheroids via isolated progenitor cells  
661 from human pluripotent stem cells. *Stem cell reports* 3: 394-403, 2014.
- 662 17. **Herlyn D, Herlyn M, Steplewski Z, and Koprowski H.** Monoclonal antibodies in  
663 cell-mediated cytotoxicity against human melanoma and colorectal carcinoma. *European*  
664 *journal of immunology* 9: 657-659, 1979.
- 665 18. **Hiemstra PS, Tetley TD, and Janes SM.** Airway and alveolar epithelial cells in  
666 culture. *The European respiratory journal* 54: 2019.
- 667 19. **Hsu JS, Zhang R, Yeung F, Tang CSM, Wong JKL, So MT, Xia H, Sham P,**  
668 **Tam PK, Li M, Wong KKY, and Garcia-Barcelo MM.** Cancer gene mutations in  
669 congenital pulmonary airway malformation patients. *ERJ open research* 5: 2019.
- 670 20. **Ishii H, Azuma K, Kinoshita T, Matsuo N, Naito Y, Tokito T, Yamada K, and**  
671 **Hoshino T.** Predictive value of CD73 expression in EGFR-mutation positive non-small-  
672 cell lung cancer patients received immune checkpoint inhibitors. *Journal of Clinical*  
673 *Oncology* 36: 9065-9065, 2018.
- 674 21. **Isomoto K, Haratani K, Hayashi H, Shimizu S, Tomida S, Niwa T, Yokoyama**  
675 **T, Fukuda Y, Chiba Y, Kato R, Tanizaki J, Tanaka K, Takeda M, Ogura T, Ishida T,**  
676 **Ito A, and Nakagawa K.** Impact of EGFR-TKI Treatment on the Tumor Immune  
677 Microenvironment in EGFR Mutation-Positive Non-Small Cell Lung Cancer. *Clinical*  
678 *cancer research : an official journal of the American Association for Cancer Research*  
679 2020.
- 680 22. **Keller MD, Nepl C, Irmak Y, Hall SR, Schmid RA, Langer R, and**  
681 **Berezowska S.** Adverse prognostic value of PD-L1 expression in primary resected  
682 pulmonary squamous cell carcinomas and paired mediastinal lymph node metastases.  
683 *Modern pathology : an official journal of the United States and Canadian Academy of*  
684 *Pathology, Inc* 31: 101-110, 2018.
- 685 23. **Kim CF, Jackson EL, Woolfenden AE, Lawrence S, Babar I, Vogel S,**  
686 **Crowley D, Bronson RT, and Jacks T.** Identification of bronchioalveolar stem cells in  
687 normal lung and lung cancer. *Cell* 121: 823-835, 2005.
- 688 24. **Kumar PA, Hu Y, Yamamoto Y, Hoe NB, Wei TS, Mu D, Sun Y, Joo LS,**  
689 **Dagher R, Zielonka EM, Wang de Y, Lim B, Chow VT, Crum CP, Xian W, and**  
690 **McKeon F.** Distal airway stem cells yield alveoli in vitro and during lung regeneration  
691 following H1N1 influenza infection. *Cell* 147: 525-538, 2011.
- 692 25. **Leach JP, and Morrissey EE.** Repairing the lungs one breath at a time: How  
693 dedicated or facultative are you? *Genes & development* 32: 1461-1471, 2018.

- 694 26. **Leblanc C, Baron M, Desselas E, Phan MH, Rybak A, Thouvenin G, Lauby C,**  
695 **and Irtan S.** Congenital pulmonary airway malformations: state-of-the-art review for  
696 pediatrician's use. *European journal of pediatrics* 176: 1559-1571, 2017.
- 697 27. **Lian S, Xie R, Ye Y, Xie X, Li S, Lu Y, Li B, Cheng Y, Katanaev VL, and Jia L.**  
698 Simultaneous blocking of CD47 and PD-L1 increases innate and adaptive cancer  
699 immune responses and cytokine release. *EBioMedicine* 42: 281-295, 2019.
- 700 28. **Litjens SH, de Pereda JM, and Sonnenberg A.** Current insights into the  
701 formation and breakdown of hemidesmosomes. *Trends in cell biology* 16: 376-383,  
702 2006.
- 703 29. **Liu Q, Liu K, Cui G, Huang X, Yao S, Guo W, Qin Z, Li Y, Yang R, Pu W,**  
704 **Zhang L, He L, Zhao H, Yu W, Tang M, Tian X, Cai D, Nie Y, Hu S, Ren T, Qiao Z,**  
705 **Huang H, Zeng YA, Jing N, Peng G, Ji H, and Zhou B.** Author Correction: Lung  
706 regeneration by multipotent stem cells residing at the bronchioalveolar-duct junction.  
707 *Nature genetics* 51: 766, 2019.
- 708 30. **Liu Q, Liu K, Cui G, Huang X, Yao S, Guo W, Qin Z, Li Y, Yang R, Pu W,**  
709 **Zhang L, He L, Zhao H, Yu W, Tang M, Tian X, Cai D, Nie Y, Hu S, Ren T, Qiao Z,**  
710 **Huang H, Zeng YA, Jing N, Peng G, Ji H, and Zhou B.** Lung regeneration by  
711 multipotent stem cells residing at the bronchioalveolar-duct junction. *Nature genetics* 51:  
712 728-738, 2019.
- 713 31. **Liu X, Liu L, Ren Z, Yang K, Xu H, Luan Y, Fu K, Guo J, Peng H, Zhu M, and**  
714 **Fu YX.** Dual Targeting of Innate and Adaptive Checkpoints on Tumor Cells Limits  
715 Immune Evasion. *Cell reports* 24: 2101-2111, 2018.
- 716 32. **Miller AJ, and Spence JR.** In Vitro Models to Study Human Lung Development,  
717 Disease and Homeostasis. *Physiology* 32: 246-260, 2017.
- 718 33. **Minor M, Alcedo KP, Battaglia RA, and Snider NT.** Cell type- and tissue-  
719 specific functions of ecto-5'-nucleotidase (CD73). *American journal of physiology Cell*  
720 *physiology* 317: C1079-C1092, 2019.
- 721 34. **Munz M, Baeuerle PA, and Gires O.** The emerging role of EpCAM in cancer and  
722 stem cell signaling. *Cancer research* 69: 5627-5629, 2009.
- 723 35. **Ng-Blichfeldt JP, de Jong T, Kortekaas RK, Wu X, Lindner M, Guryev V,**  
724 **Hiemstra PS, Stolk J, Konigshoff M, and Gosens R.** TGF-beta activation impairs  
725 fibroblast ability to support adult lung epithelial progenitor cell organoid formation.  
726 *American journal of physiology Lung cellular and molecular physiology* 317: L14-L28,  
727 2019.
- 728 36. **Park LC, Rhee K, Kim WB, Cho A, Song J, Anker JF, Oh M, Bais P, Namburi**  
729 **S, Chuang J, and Chae YK.** Immunologic and clinical implications of CD73 expression  
730 in non-small cell lung cancer (NSCLC). *Journal of Clinical Oncology* 36: 12050-12050,  
731 2018.
- 732 37. **Picher M, Burch LH, Hirsh AJ, Spsychala J, and Boucher RC.** Ecto 5'-  
733 nucleotidase and nonspecific alkaline phosphatase. Two AMP-hydrolyzing ectoenzymes  
734 with distinct roles in human airways. *The Journal of biological chemistry* 278: 13468-  
735 13479, 2003.
- 736 38. **Prasad M, Kumar B, Bhat-Nakshatri P, Anjanappa M, Sandusky G, Miller KD,**  
737 **Storniolo AM, and Nakshatri H.** Dual TGFbeta/BMP Pathway Inhibition Enables  
738 Expansion and Characterization of Multiple Epithelial Cell Types of the Normal and  
739 Cancerous Breast. *Molecular cancer research : MCR* 17: 1556-1570, 2019.

- 740 39. **Ray S, Chiba N, Yao C, Guan X, McConnell AM, Brockway B, Que L,**  
741 **McQualter JL, and Stripp BR.** Rare SOX2+ Airway Progenitor Cells Generate KRT5+  
742 Cells that Repopulate Damaged Alveolar Parenchyma following Influenza Virus  
743 Infection. *Stem cell reports* 7: 817-825, 2016.
- 744 40. **Salwig I, Spitznagel B, Vazquez-Armendariz AI, Khalooghi K, Guenther S,**  
745 **Herold S, Szibor M, and Braun T.** Bronchioalveolar stem cells are a main source for  
746 regeneration of distal lung epithelia in vivo. *The EMBO journal* 38: 2019.
- 747 41. **Samanta D, Park Y, Ni X, Li H, Zahnow CA, Gabrielson E, Pan F, and**  
748 **Semenza GL.** Chemotherapy induces enrichment of CD47(+)/CD73(+)/PDL1(+)  
749 immune evasive triple-negative breast cancer cells. *Proceedings of the National*  
750 *Academy of Sciences of the United States of America* 115: E1239-E1248, 2018.
- 751 42. **Sidders B, Zhang P, Goodwin K, O'Connor G, Russell DL, Borodovsky A,**  
752 **Armenia J, McEwen R, Linghu B, Bendell JC, Bauer TM, Patel MR, Falchook GS,**  
753 **Merchant M, Pouliot G, Barrett JC, Dry JR, Woessner R, and Sachsenmeier K.**  
754 Adenosine Signaling Is Prognostic for Cancer Outcome and Has Predictive Utility for  
755 Immunotherapeutic Response. *Clinical cancer research : an official journal of the*  
756 *American Association for Cancer Research* 26: 2176-2187, 2020.
- 757 43. **Stocker JT, Madewell JE, and Drake RM.** Congenital cystic adenomatoid  
758 malformation of the lung. Classification and morphologic spectrum. *Human pathology* 8:  
759 155-171, 1977.
- 760 44. **Swarr DT, Peranteau WH, Pogoriler J, Frank DB, Adzick NS, Hedrick HL,**  
761 **Morley M, Zhou S, and Morrisey EE.** Novel Molecular and Phenotypic Insights into  
762 Congenital Lung Malformations. *American journal of respiratory and critical care*  
763 *medicine* 2018.
- 764 45. **Toufen C, Jr., Costa EL, Hirota AS, Li HY, Amato MB, and Carvalho CR.**  
765 Follow-up after acute respiratory distress syndrome caused by influenza a (H1N1) virus  
766 infection. *Clinics (Sao Paulo)* 66: 933-937, 2011.
- 767 46. **Trzpis M, McLaughlin PM, de Leij LM, and Harmsen MC.** Epithelial cell  
768 adhesion molecule: more than a carcinoma marker and adhesion molecule. *The*  
769 *American journal of pathology* 171: 386-395, 2007.
- 770 47. **Turcotte M, Spring K, Pommey S, Chouinard G, Cousineau I, George J,**  
771 **Chen GM, Gendoo DM, Haibe-Kains B, Karn T, Rahimi K, Le Page C, Provencher**  
772 **D, Mes-Masson AM, and Stagg J.** CD73 is associated with poor prognosis in high-  
773 grade serous ovarian cancer. *Cancer research* 75: 4494-4503, 2015.
- 774 48. **Vaughan AE, Brumwell AN, Xi Y, Gotts JE, Brownfield DG, Treutlein B, Tan**  
775 **K, Tan V, Liu FC, Looney MR, Matthay MA, Rock JR, and Chapman HA.** Lineage-  
776 negative progenitors mobilize to regenerate lung epithelium after major injury. *Nature*  
777 517: 621-625, 2015.
- 778 49. **Wang L, Dorn P, Zeinali S, Froment L, Berezowska S, Kocher GJ, Alves MP,**  
779 **Brugger M, Esteves BIO, Blank F, Wotzkow C, Steiner S, Amacker M, Peng RW,**  
780 **Marti TM, Guenat OT, Bode PK, Moehrlen U, Schmid RA, and Hall SRR.**  
781 CD90(+)/CD146(+) identifies a pulmonary mesenchymal cell subtype with both immune  
782 modulatory and perivascular-like function in postnatal human lung. *American journal of*  
783 *physiology Lung cellular and molecular physiology* 318: L813-L830, 2020.
- 784 50. **Xi Y, Kim T, Brumwell AN, Driver IH, Wei Y, Tan V, Jackson JR, Xu J, Lee**  
785 **DK, Gotts JE, Matthay MA, Shannon JM, Chapman HA, and Vaughan AE.** Local



786 lung hypoxia determines epithelial fate decisions during alveolar regeneration. *Nature*  
787 *cell biology* 19: 904-914, 2017.  
788 51. **Zaragosi LE, Deprez M, and Barbry P.** Using single-cell RNA sequencing to  
789 unravel cell lineage relationships in the respiratory tract. *Biochemical Society*  
790 *transactions* 48: 327-336, 2020.  
791 52. **Zunder ER, Lujan E, Goltsev Y, Wernig M, and Nolan GP.** A continuous  
792 molecular roadmap to iPSC reprogramming through progression analysis of single-cell  
793 mass cytometry. *Cell stem cell* 16: 323-337, 2015.

794

795 **Figure Legends**

796 **Figure 1. EpCAM<sup>+</sup> cells enriched for CD73 found in both respiratory epithelium**

797 **and alveolar region of postnatal lung.** (A) Illustration of approach to identify and

798 characterize epithelial cell subsets in human lung. (B-C) Representative flow plots are

799 shown. (D) Scatter plots show percentage of cell subsets within EpCAM<sup>+</sup> fraction (gate

800 R4) after subgating for CD73 and CD90 in postnatal lung. (E) Scatter plots comparing

801 EpCAM<sup>+</sup>CD73<sup>+</sup> cell subset in postnatal versus adult human lung. N = 19, biological

802 replicates for postnatal lung; N = 15, biological replicates for adult lung. (F, H)

803 Hematoxylin and Eosin (H&E) stained unaffected postnatal lung. (G, I) Immunostaining

804 of postnatal lung showing EpCAM (red) cells co-expressing CD73 (green, white arrow)

805 in respiratory epithelium (G) and alveolar region (I). In the alveolus, CD73 cells lacking

806 EpCAM are also found (white arrowhead). Nuclei were counterstained with DAPI. Br,

807 bronchiole; Alv, alveolar; Lu, bronchiolar lumen. Scale bars 30 μm (G) and 20 μm (I).

808 Data are presented as mean ± SD. Error bars show SD. *P* values are shown in the

809 figure.

810

811 **Figure 2. EpCAM<sup>+</sup>CD73<sup>+</sup> cells are basal cell-like after expansion in culture.** (A)

812 Diagram of assay to expand prospectively isolated EpCAM<sup>+</sup>CD73<sup>+</sup> cells. Phase contrast

813 image of cells after reaching confluence. (B) mRNA levels of genes marking proximal

814 and distal airway cells and markers of basal stem cells, alveolar type II and type I cells in

815 FACS-sorted EpCAM<sup>+</sup>CD73<sup>+</sup> cells by RT-qPCR. Upper airway (n = 3, biological

816 replicates), postnatal lung tissue (n = 5, biological replicates) and EpCAM<sup>+</sup>CD73<sup>+</sup> cells

817 (n = 9, biological replicates). Gene expression level in postnatal lung tissue is set at one.

818 Representative immunofluorescence stains of FACS-sorted EpCAM<sup>+</sup>CD73<sup>+</sup> cells (C, D)

819 and their quantification (E) after reaching confluence in culture (n = 3, biological  
820 replicates). Scale bar 50  $\mu\text{m}$  (C, D). (F) Representative FACS plots demonstrating that  
821 HTII-280 marks a minor subset of EpCAM<sup>+</sup>CD73<sup>+</sup> progenitor cells (gate R6). (G) Scatter  
822 plots showing co-expression of CD24 and PDPN. (postnatal, n = 6, biological replicates;  
823 adult, n = 7, biological replicates). (H) Schematic depicting the different cell subsets  
824 found within the EpCAM<sup>+</sup>CD73<sup>+</sup> fraction after expansion in culture. Data are presented  
825 as mean  $\pm$  SD. Error bars show SD. \**P* < 0.05; ns, not significant; ND, not detected.

826

827 **Figure 3. Disrupting epithelial NOTCH signaling alters mucociliary-secretory cell**  
828 **fate of EpCAM<sup>+</sup>CD73<sup>+</sup> cells.** (A) Representative hematoxylin and eosin (H&E) stain of  
829 unaffected lung showing normal bronchiole (Br) and surrounding alveolar region (Alv).  
830 (B) Immunostaining postnatal lung for TRP63 (red) and KRT5 (green). Higher-power  
831 view of boxed area shows dual positive TRP63-KRT5 cells (white arrow) and single  
832 positive TRP63 cells (white arrowhead) along the basal membrane. Nuclei were  
833 counterstained with DAPI. (C) Immunostaining postnatal lung for EpCAM (red), SOX2  
834 (white) and KRT5 (green). Higher power view of boxed area shows single layer of KRT5  
835 cells lining basal membrane. Nuclei were counterstained with DAPI. Br, bronchi; Alv,  
836 alveolar region. Scale bars 500  $\mu\text{m}$  (A), 100  $\mu\text{m}$  (B-C). Diagram of 2D air-liquid-interface  
837 (ALI) using either postnatal (D) or adult (F) EpCAM<sup>+</sup>CD73<sup>+</sup> cells to examine the role of  
838 the NOTCH signaling pathway in airway differentiation. (D, F) Representative Z-stacks  
839 (upper panel: xy-projection; lower panel zy-projection) through different planes of ALI  
840 membranes showing formation of a pseudostratified mucociliary epithelium and impact  
841 of DLL4 (10 ng/ml) or DAPT (10  $\mu\text{M}$ ) on proximal airway differentiation. Ciliated ( $\beta$ -  
842 tubulin, yellow) and goblet cells (MUC5AC, white) can be found at the apical surface

843 (apical xy plane). Images through the middle xy plane showing club cells (SCGB1A1,  
844 purple) together with E-cadherin (Ecad, green) showing changes in cell shape (white  
845 arrow). At the basal xy plane, representative images showing basal cells (TRP63, red).  
846 (E, G) 3D volume reconstruction of 2D differentiation at ALI to enable visualization basal  
847 cells (TRP63, red). n = 3, biological replicates. Scale bars: 500  $\mu\text{m}$  (A), 100  $\mu\text{m}$  (B, C),  
848 30  $\mu\text{m}$  (D, F).

849

850 **Figure 4. EpCAM<sup>+</sup>CD73<sup>+</sup> cells generate lung organoids recapitulating a**  
851 **mucociliary-secretory cell fate found *in vivo*.** (A) Diagram of 3D airway organoid  
852 assay using EpCAM<sup>+</sup>CD73<sup>+</sup> cells. (B) Transmission electron microscopy shows  
853 ultrastructural analysis of an individual organoid generated from postnatal (top) or adult  
854 (bottom) EpCAM<sup>+</sup>CD73<sup>+</sup> cells. n=2, biological replicates. CC, ciliated cell; CR, ciliary  
855 rootlet; CZ, contact zone; NSC, nucleus of secretory cell; SC, secretory cell; SG,  
856 secretory granules. (C) mRNA levels of genes expressed by airway organoids using RT-  
857 qPCR. n=4, biological replicates. Gene expression level in postnatal lung tissue is set at  
858 one. (D) Diagram of 3D alveolar organoid assay using EpCAM<sup>+</sup>CD73<sup>+</sup> cells. Phase  
859 contrast image (4X) showing generation of organoid structures (right panel). (E)  
860 Representative immunofluorescence image of single alveolar organoids. Z stack  
861 showing saccule-like features, multicellular organization and lumen formation is  
862 highlighted. E-cadherin (red) is used to identify epithelial saccule-like structures and ATI  
863 cells stained for proSPC (green, white arrow) are shown. (F) Z-stack of an individual  
864 organoid showing KRT5<sup>+</sup> cells and the location of ATI cells using the marker HOPX.  
865 Magnified Z-axis shows the location of HOPX<sup>+</sup> cells facing in towards the lumen of the  
866 organoid. Nuclei were counterstained with DAPI (blue). Scale bars: 50  $\mu\text{m}$  (E, F). Two of

867 three independent experiments are shown. (G) Representative FACS plot of alveolar  
868 organoids showing expression of CD73 and HTII-280 gated from EpCAM<sup>+</sup> cells (left  
869 panel) and isotype for HTII-280 (right panel). (H) Scatter plots show percent of cell  
870 subsets within EpCAM<sup>+</sup> fraction after subgating for CD73 and HTII-280. (I-J) Scatter  
871 plots showing percent of cell subsets within CD73<sup>+</sup>HTII-280<sup>-</sup> (I) or CD73<sup>+</sup>HTII-280<sup>+</sup>  
872 fraction (J) after subgating for CD24 and PDPN. Data are presented as mean ± SD. \**P* <  
873 0.05; \*\**P* < 0.01.

874

875 **Figure 5. Cystic lung lesions lined with EpCAM<sup>+</sup>CD73<sup>+</sup> cells.** (A-D) Histological  
876 analysis of unaffected postnatal lung tissue (A) and congenital lung lesions (B-D).  
877 Bottom panels show boxed area at higher power. (E,G,I) Histological analysis (F,H,J)  
878 and immunostaining of CPAM (F), Chronic bronchiolitis (H) and CPAM (J) with EpCAM  
879 (green) and CD73 (red). Right panels show higher-power view of boxed area and single  
880 channels separated without DAPI to highlight co-stained cells. Nuclei are counterstained  
881 with DAPI (blue). Br, bronchiole; Alv, alveolar region; Lu, bronchiolar lumen. Scale bars:  
882 500 μm (G), 200 μm (A-D, E, I); 100 μm (F,H,J).

883

884 **Figure 6. Expansion in EpCAM<sup>+</sup>SCGB1A1<sup>+</sup> and EpCAM<sup>+</sup>proSPC<sup>+</sup> cells in distal**  
885 **lung compartment in congenital lesions and other airway abnormalities.**  
886 Immunostaining shows cystic structures stained with EpCAM (red), SCGB1A1 (white)  
887 and proSPC (green) in CPAM (A, C) and lobar emphysema (E). (B,D,F) Right panels of  
888 higher-power view of boxed area highlight regions of dual positive EpCAM-SCGB1A1  
889 (yellow arrowhead) or EpCAM-proSPC (yellow arrow) stained cells. Channels are  
890 separated to show single stained cells. Br, bronchiole; Alv, alveolar region; Lu,

891 bronchiolar lumen. Scale bars: 100  $\mu\text{m}$  (A,B,C,E,F); 50  $\mu\text{m}$  (D),. Nuclei are  
892 counterstained with DAPI (blue). (G) Increase in  $\text{EpCAM}^+\text{proSPC}^+$  and  
893  $\text{EpCAM}^+\text{SCGB1A1}^+$  cells per total number of  $\text{EpCAM}^+$  cells in disease compared with  
894 healthy area of lung. Data presented as mean  $\pm$  SD,  $n = 3$ , biological replicates.

895  
896 **Figure 7. Re-emergence of  $\text{EpCAM}^+\text{CD73}^+$  cells in NSCLC coincides with**  
897 **increased expression of immune checkpoints and poor prognosis.** (A,C)  
898 Hematoxylin and Eosin (H&E) staining of tumor specimen. (B) Higher-power view of  
899 boxed area from (A) shows dual positive  $\text{EpCAM}$  (green) and  $\text{CD73}$  (Red) staining tumor  
900 islands (Tu) (B). (D) Serial section showing the nuclei of dual positive  $\text{EpCAM-CD73}$   
901 tumor cells stain for TRP63 (red). Channels are separated to show single stained cells.  
902 (E-F) Scatter plots show frequency of  $\text{EpCAM}^+$  tumor cells enriched for  $\text{CD73}$  in (E)  
903 LUAD ( $n = 64$ ) and (F) LUSC ( $n = 58$ ). (G-H) Scatter plots showing the mean  
904 fluorescence intensity (MFI) for PD-L1 and CD47 on  $\text{EpCAM}^+\text{CD73}^+$  cell subset in (F)  
905 LUAD ( $n = 56 - 64$ ) and (H) LUSC ( $n = 49 - 57$ ). All data determined by flow cytometry.  
906  $*P < 0.05$ ;  $***P < 0.0001$ ; ns, not significant. (I) Representative images of PD-L1 and  
907 CD47 expression in serial sections from a single LUAD or LUSC patient. Scale bars: 500  
908  $\mu\text{m}$  (C), 200  $\mu\text{m}$  (A, B.), 100  $\mu\text{m}$  (D), 50  $\mu\text{m}$  (I).

909  
910 **DOI:10.6084/m9.figshare.12488867**

**Figure 1**

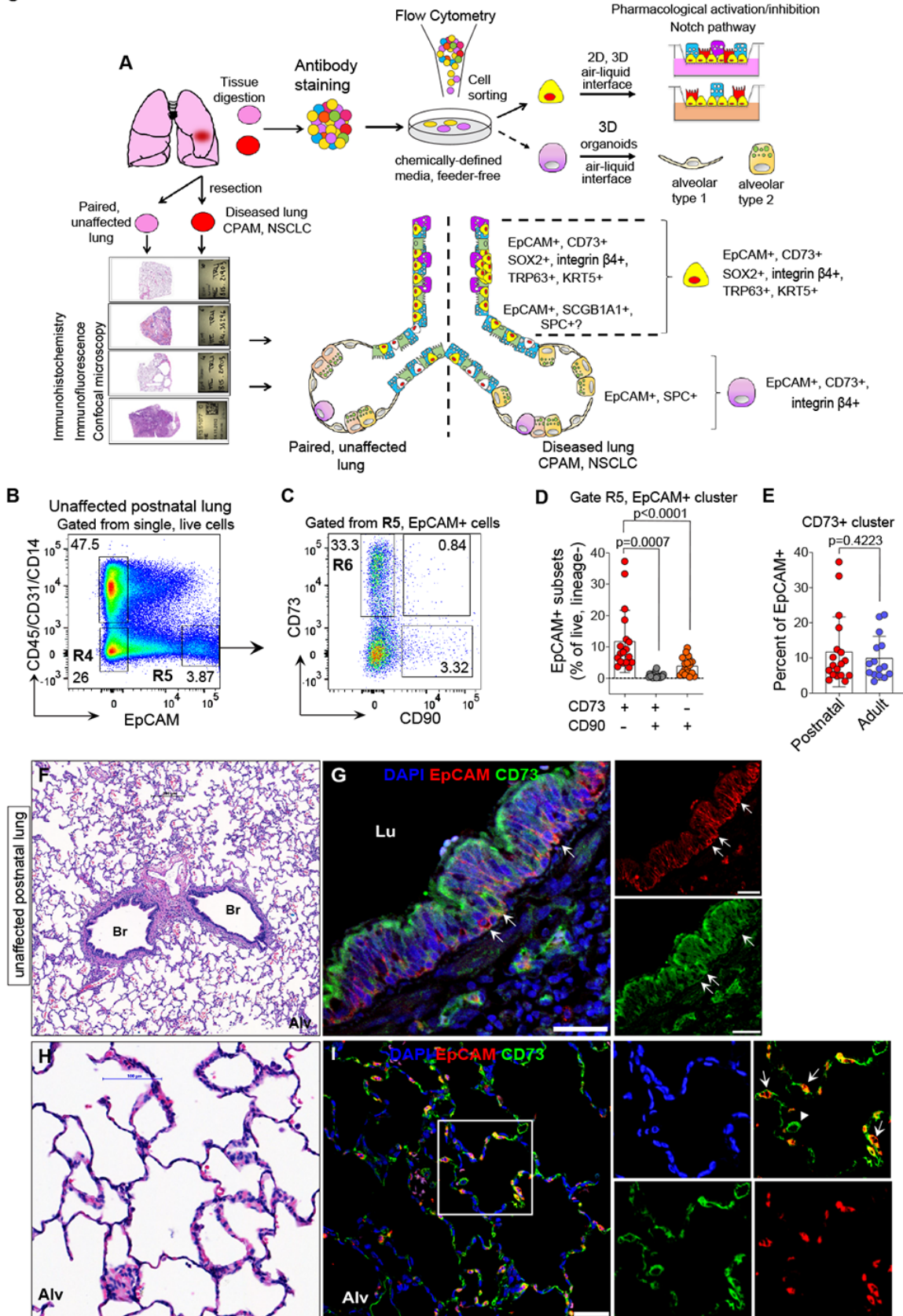


**Figure 2**

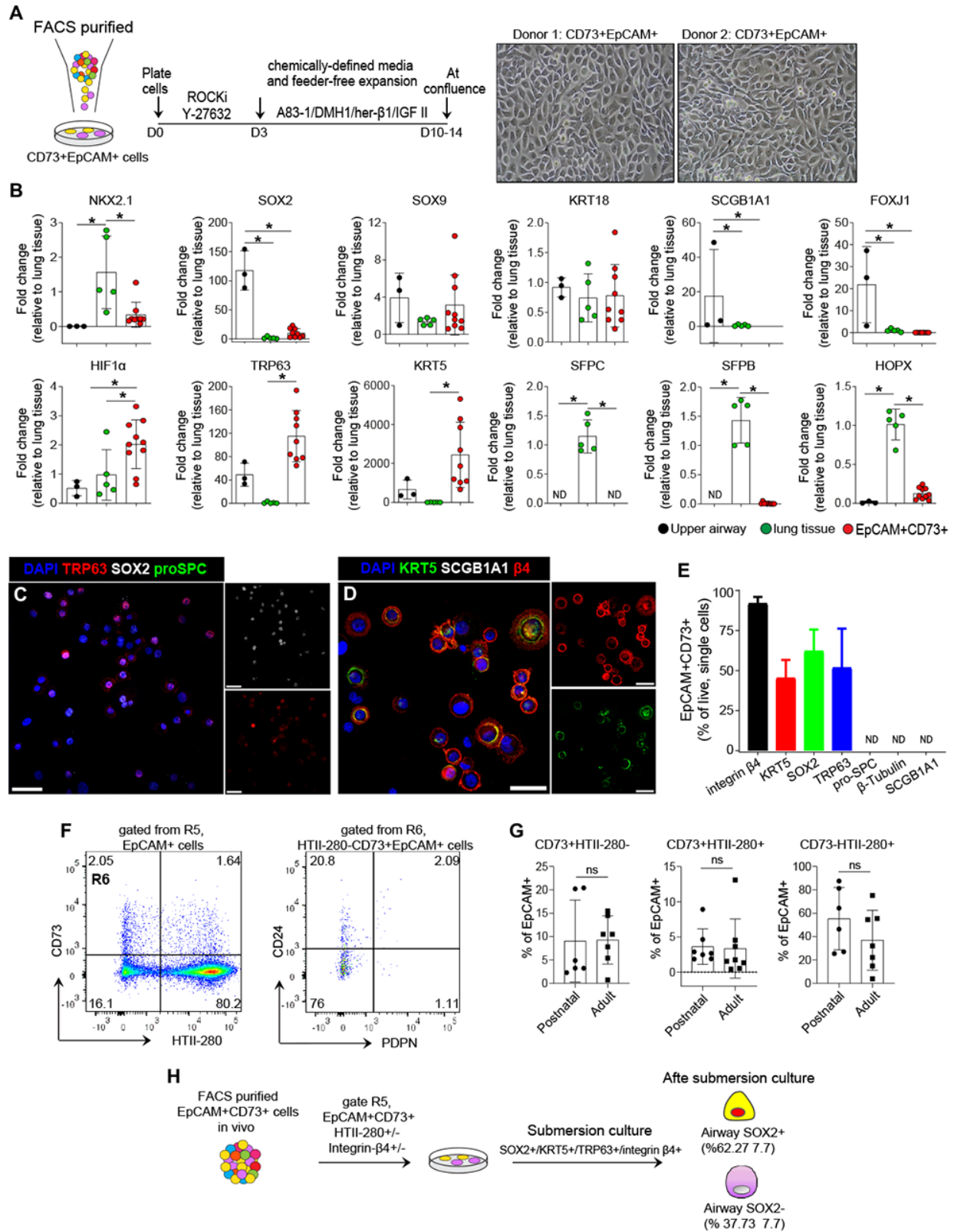




**Figure 3**

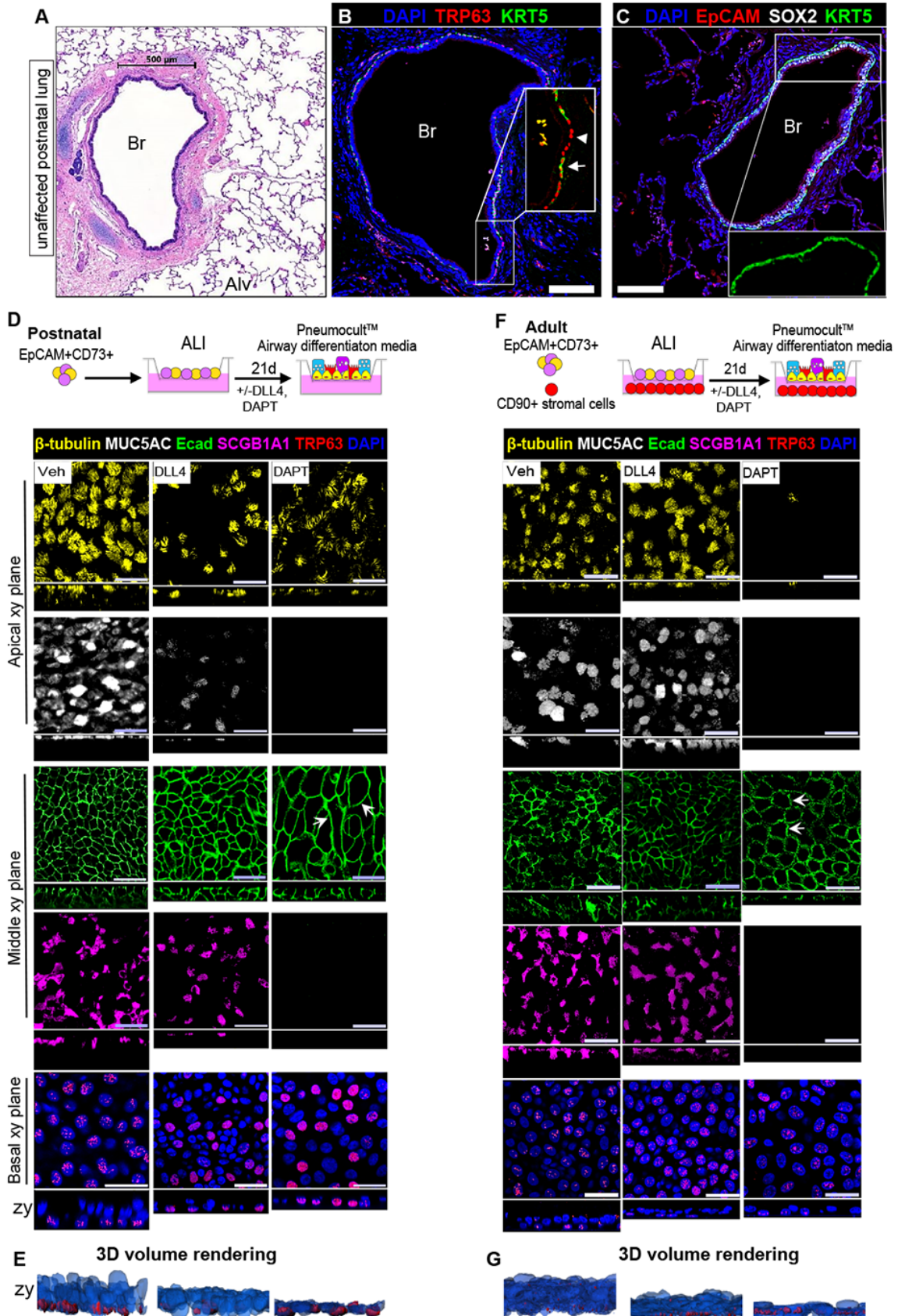


**Figure 4**

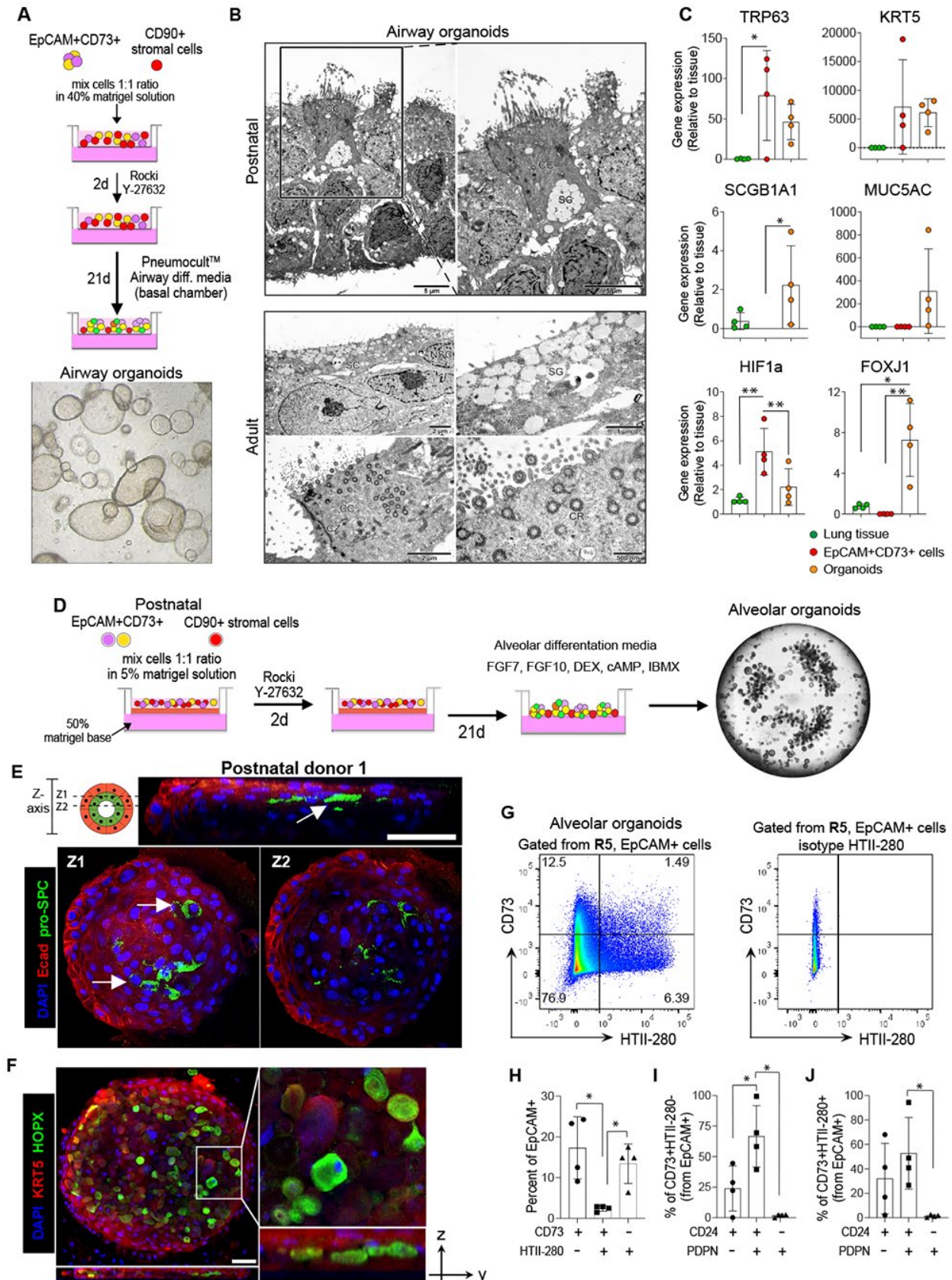


Figure 5

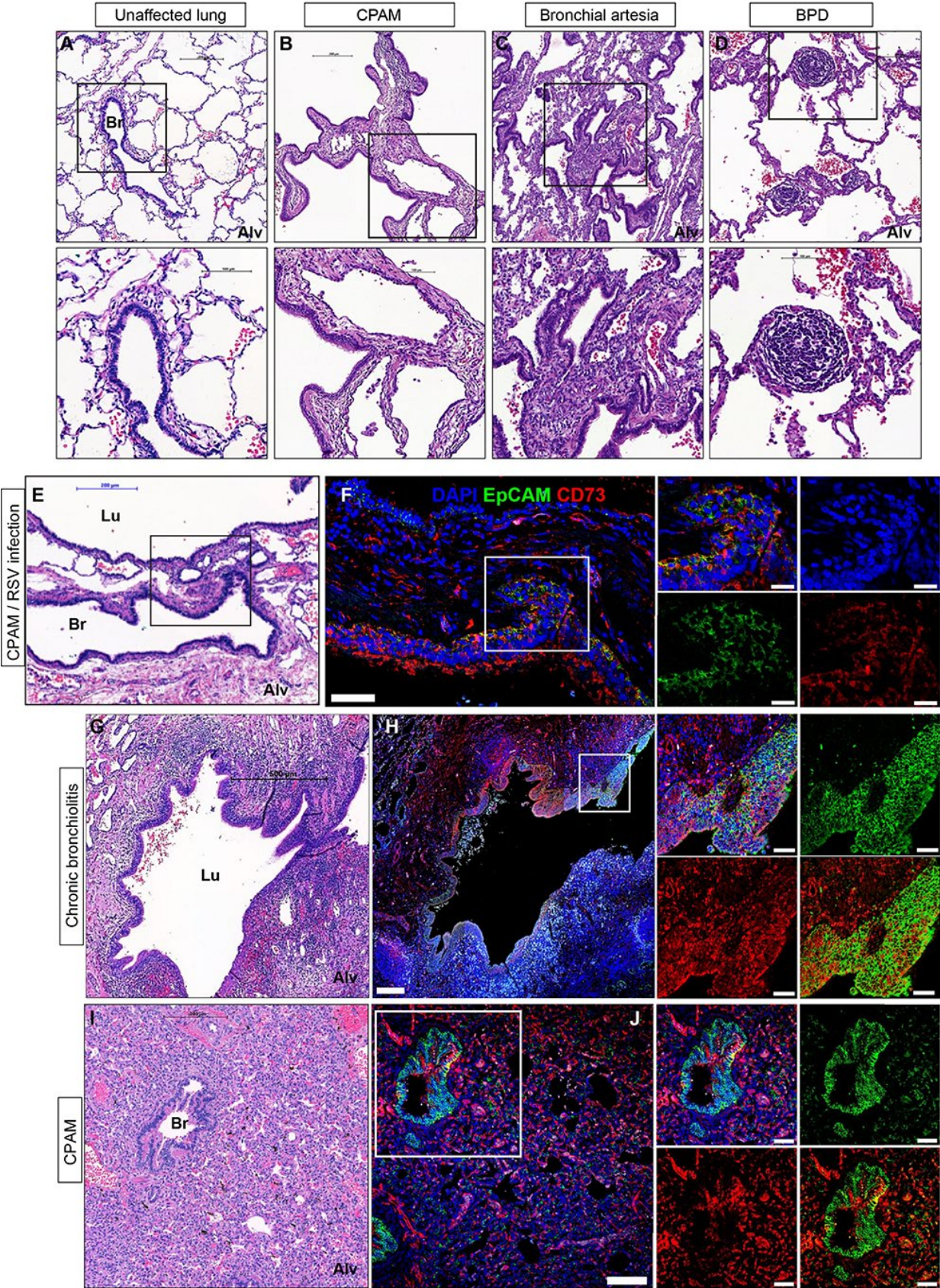


Figure 6

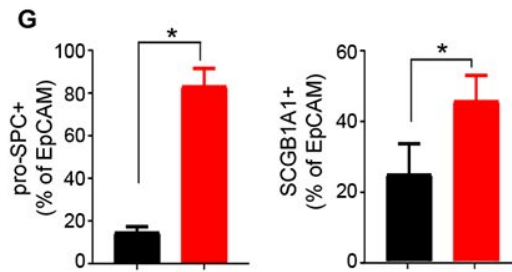
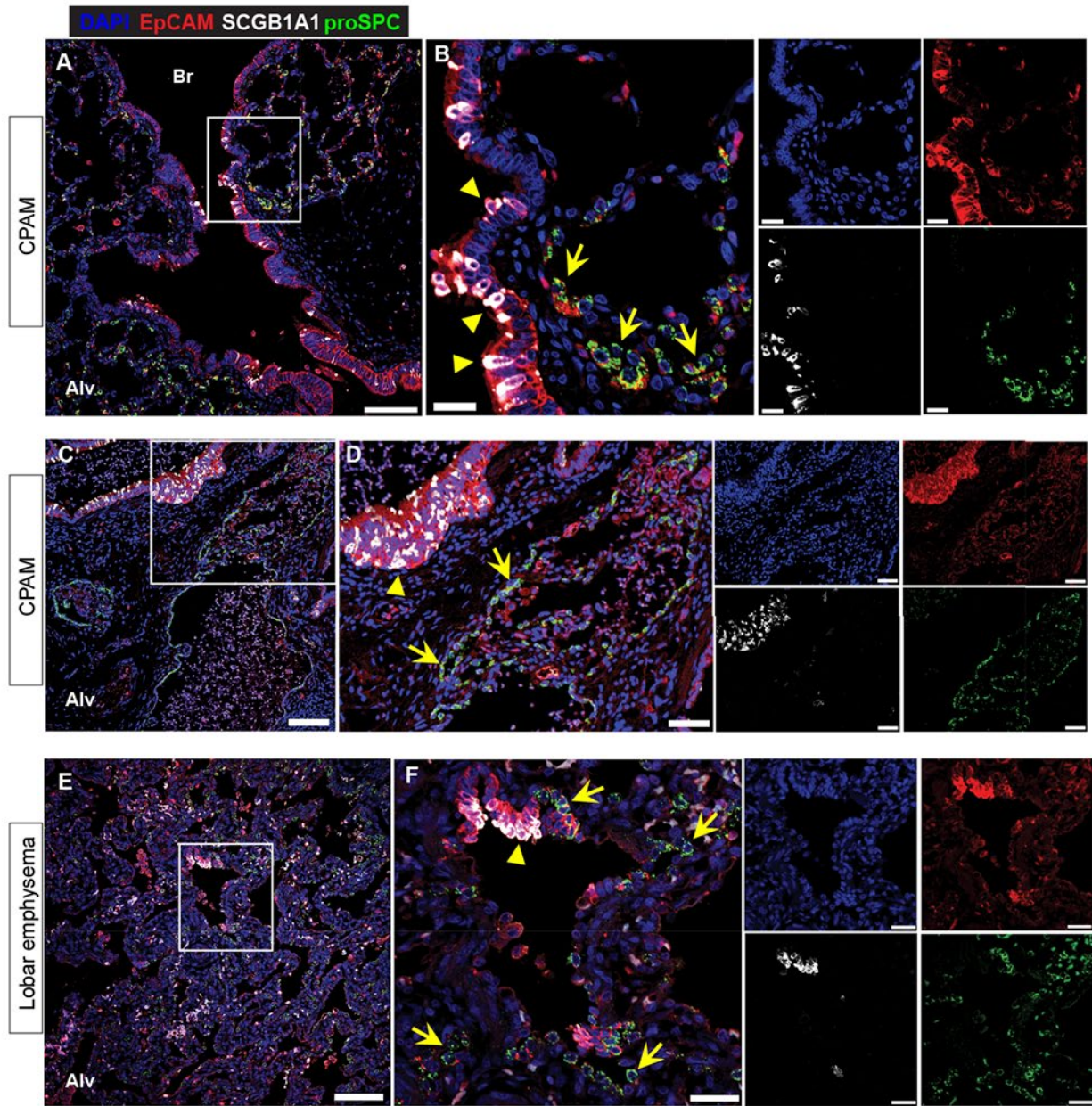


Figure 7

